Statistical Dynamics of Spatial-Order Formation by Communicating Cells

Pavinato Olimpio, E.; Dang, Yiteng; Youk, Hyun

DOI
10.1016/j.isci.2018.03.013

Publication date
2018

Document Version
Final published version

Published in
iScience

iScience

CellPress

Article

Statistical Dynamics of Spatial-Order Formation by Communicating Cells

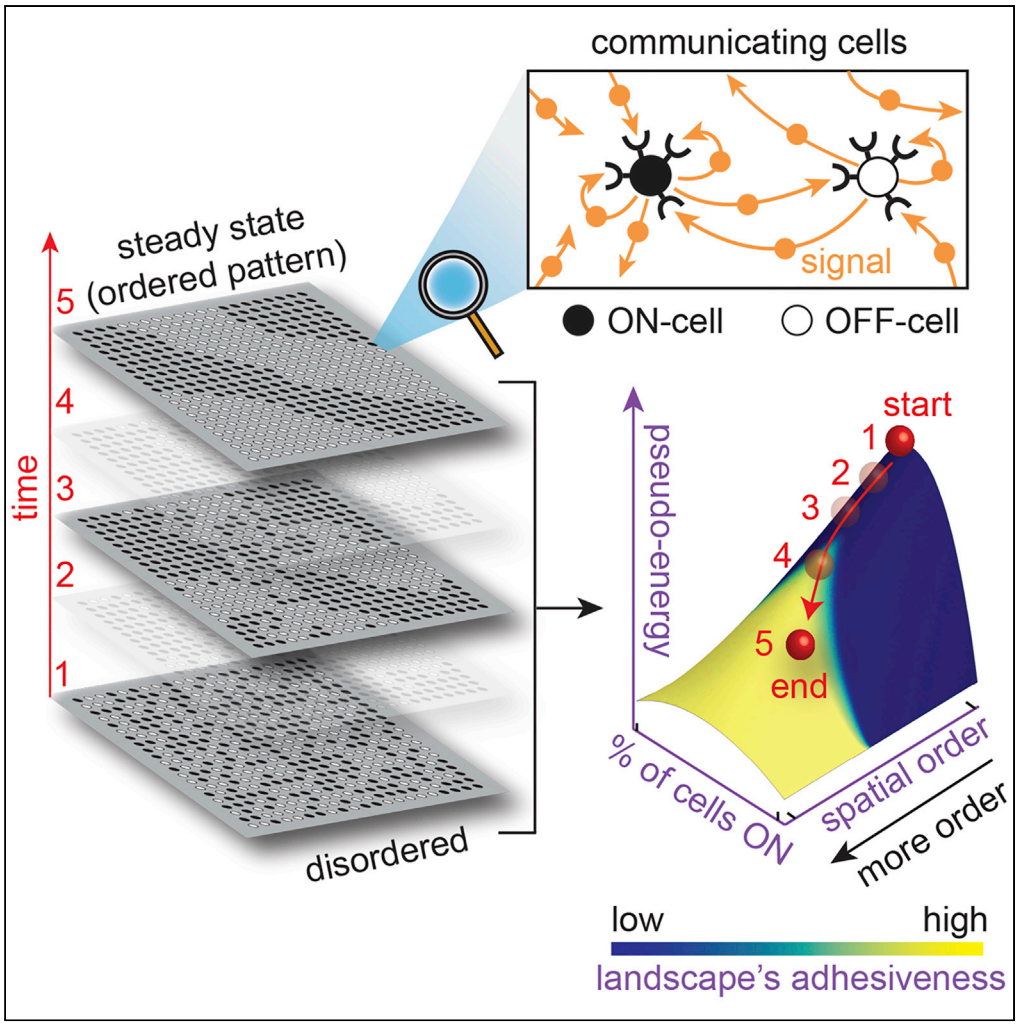

Eduardo P. Olimpio, Yiteng Dang, Hyun Youk

h.youk@tudelft.nl

HIGHLIGHTS

Field of communicating, secrete-and-sense cells form spatial patterns

Particle rolling down a "pseudo-energy landscape" models pattern-formation dynamics

Equation of motion describes the particle's motion and hence pattern formation

This statistical mechanics-type framework applies to other forms of communication

Olimpio et al., iScience 2, 27–40
April 27, 2018
https://doi.org/10.1016/j.isci.2018.03.013

iScience

CellPress

Article

Statistical Dynamics of Spatial-Order Formation by Communicating Cells

Eduardo P. Olimpio,[1,2,3] Yiteng Dang,[1,2,3] and Hyun Youk[1,2,4,*]

SUMMARY

Communicating cells can coordinate their gene expressions to form spatial patterns, generating order from disorder. Ubiquitous "secrete-and-sense cells" secrete and sense the same molecule to do so. Here we present a modeling framework—based on cellular automata and mimicking approaches of statistical mechanics—for understanding how secrete-and-sense cells with bistable gene expression, from disordered beginnings, can become spatially ordered by communicating through rapidly diffusing molecules. Classifying lattices of cells by two "macrostate" variables—"spatial index," measuring degree of order, and average gene-expression level—reveals a conceptual picture: a group of cells behaves as a single particle, in an abstract space, that rolls down on an adhesive "pseudo-energy landscape" whose shape is determined by cell-cell communication and an intracellular gene-regulatory circuit. Particles rolling down the landscape represent cells becoming more spatially ordered. We show how to extend this framework to more complex forms of cellular communication.

INTRODUCTION

Cells can communicate by secreting signaling molecules, and this often underlies their collective behaviors. A striking example is that of initially uncoordinated cells, through cell-cell communication, coordinating their gene expressions to generate spatial patterns or structures (Gregor et al., 2010; Sawai et al., 2005; Danino et al., 2010; Liu et al., 2011). Many cells partly or completely control such "disorder-to-order" dynamics by simultaneously secreting and sensing the same signaling molecule (Doğaner et al., 2016; Youk and Lim, 2014a). These "secrete-and-sense cells" appear across diverse organisms and include quorum-sensing social ameba, *Dictyostelium discoideum*, that form fruiting bodies (Gregor et al., 2010; Sawai et al., 2005; Sgro et al., 2015) and autocrine-signaling T cells (Antebi et al., 2013; Sporn and Todaro, 1980; Youk and Lim, 2014b). Based on mounting evidence from studies of various organisms (Gregor et al., 2010; Danino et al., 2010; Youk and Lim, 2014a; Antebi et al., 2013; Mehta et al., 2009; Kamino et al., 2017; Hart et al., 2014; De Monte et al., 2007; Umeda and Inouye, 2004; You et al., 2004; Pai et al., 2012; Coppey et al., 2007; Shvartsman et al., 2001), researchers now suspect that secrete-and-sense cells, many of which are governed by the same type of genetic circuit (Doğaner et al., 2016), are highly suited for spatially coordinating their gene expressions. However, if true, exactly why this is so, whether there are common design principles shared by the different organisms, what the dynamics underlying their disorder-to-order transition is, and how to even quantify their spatial order remain open questions. In this article, we address these questions in the context of initially disordered fields of secrete-and-sense cells that self-organize into spatially ordered fields without any pre-existing morphogens. Specifically, we develop a theoretical framework that takes a simple and ubiquitous class of secrete-and-sense cells, sensibly defines and quantifies the notion of the cells' spatial order, and then elucidates how the spatial order evolves over time. We focus here on analytically describing how spatial correlations among cells' gene-expression levels dynamically emerge rather than on describing the shapes, sizes, and formations of specific spatial patterns (e.g., stripes). To study how these cells generate specific patterns, one often uses exhaustive numerical simulations that are adapted to particular settings (Cotterell and Sharpe, 2010; Cotterell et al., 2015; Chen et al., 2015). Although such simulations provide insights into the dynamics of spatial-order formation, a different modeling framework may provide complementary insights that are difficult to extract from the often large numbers of parameters involved in numerical simulations.

Our main idea is that describing hundreds to thousands of secrete-and-sense cells forming a particular spatial configuration is infeasible without exhaustive numerical simulations but that it is possible to analytically describe how an ensemble of "similar" spatial configurations evolves over time without knowing the state of every single cell. As we will show, we do this by defining quantities that are similar to those found in statistical physics but have meanings and properties that are very different and are adapted for describing

[1]Kavli Institute of Nanoscience, Delft University of Technology, Delft, the Netherlands

[2]Department of Bionanoscience, Delft University of Technology, Delft 2629HZ, the Netherlands

[3]These authors contributed equally

[4]Lead Contact

*Correspondence: h.youk@tudelft.nl

https://doi.org/10.1016/j.isci.2018.03.013

cells. Specifically, we will define a "spatial index"—a number whose magnitude is between zero (complete disorder) and one (complete order). Inspired by approaches of statistical mechanics, we will group all lattices of cells that have the same spatial order parameter and average gene-expression level into an ensemble that we will call a "macrostate." Surprisingly, we find that this macrostate moves like a particle that drifts and diffuses in an abstract, two-dimensional space that we will call a "phase space"—since it describes all possible spatial configurations of the lattice—and whose coordinates denote the cells' spatial order and average gene-expression level. We find that the particle, representing an entire cellular lattice, moves in the phase space by rolling down on a "pseudo-energy landscape," which is a visual landscape that is shaped by communication among the cells and the intracellular gene-regulatory circuit that controls how the cells secrete and sense the molecule. We will show that the shape of this landscape is quantitatively defined by a function that we will call "pseudo-energy" and show that although it mathematically resembles the Hamiltonian of the Ising model, it has different properties. We will show that the gradient of the pseudo-energy and a "trapping probability," which quantifies the adhesiveness of the pseudo-energy landscape, together determine the particle's trajectories in the phase space—the particle rolls down along the negative of the gradient of the pseudo-energy, and at locations where the landscape is highly adhesive, it halts. Crucially, we will show that these trapping locations on the pseudo-energy landscape—the locations where the particle halts—correspond to highly ordered spatial configurations such as islands of cells that have the same gene-expression level. A moderate amount of noise can induce the particle to roll down further on the pseudo-energy landscape, and this corresponds to the cells forming patterns with even higher spatial organizations. We thus provide here an intuitive and visual picture, based on experimentally attainable quantities, that is both practical and conceptual for elucidating how a simple class of secrete-and-sense cells spatially coordinate their gene expressions. We will also show that this modeling framework is extendable to more complex forms of cell-cell communication, including those involving more than one type of signaling molecule and multiple cell types.

RESULTS

Cellular Automaton Simulates Secrete-and-Sense Cells that Slowly Respond to a Rapidly Diffusing Signaling Molecule

We used a cellular automaton (Ermentrout and Edelstein-Keshet, 1993) to simulate secrete-and-sense cells. We will compare the results of the cellular automaton with our theory's predictions. We considered a two-dimensional, triangular lattice of N spherical, immobile secrete-and-sense cells of radius R and a lattice spacing a_o. As a proof of principle, we considered "simple" secrete-and-sense cells, which we define to be cells (1) that very slowly respond to their fast diffusing signal and (2) whose gene-expression level, which is determined by the extracellular concentration of the signal and signal-secretion rate, exhibit switch-like (digital) bistability (see Supplemental Information section S1). These two features were motivated by experimentally characterized secrete-and-sense cells. Examples include yeasts that secrete and sense a mating pheromone in a nearly digital manner (diffusion timescale ~1 s; response timescale ~30 min) (Youk and Lim, 2014a; Rappaport and Barkai, 2012) and mouse hair follicles, which are secrete-and-sense organs that act as digital secrete-and-sense cells on a triangular lattice (diffusion timescale ~12 hr; response timescale ~1.5 days) (Chen et al., 2015; Maire and Youk, 2015a) (see also Table S1). Each cell's gene expression is either "ON" (when its signal-secretion rate is at a maximum) or "OFF" (when its signal-secretion rate is at a minimum, basal level). Each cell senses a steady-state signal concentration c on itself. If c is higher (lower) than a threshold concentration K, which we call an "activation threshold," then the cell is ON (OFF). When N = 1, the lone ON-cell (OFF-cell) maintains a steady-state concentration C_{ON} (C_{OFF}) on itself. We set C_{OFF} = 1 so that we express all concentrations as multiples of C_{OFF}. Our cellular automaton computes the concentration on every cell, then synchronously updates each cell's state, and then repeats this process until the cellular lattice reaches a steady-state configuration in which no cell's state requires an update. By running the cellular automaton on randomly distributed ON- and OFF-cells, we observed that initially disordered lattices could indeed evolve into spatially ordered steady-state configurations such as islands of ON-cells (Figure 1A) (Maire and Youk, 2015b).

Secrete-and-Sense Cells Can Be Classified Into Distinct Behavioral Phases

To reveal how the disorder-to-order dynamics arises, we will analyze the cellular automaton in each of the cells' "behavioral phases" that we described in a previous work (Figure 1B; details in Supplemental Information section S1) (Maire and Youk, 2015b). As the previous work showed, the behavioral phases represent how one cell turns on/off another cell. They arise from self-communication (i.e., a cell captures its own signal) competing with neighbor communication (i.e., a cell captures the other cells' signal). The

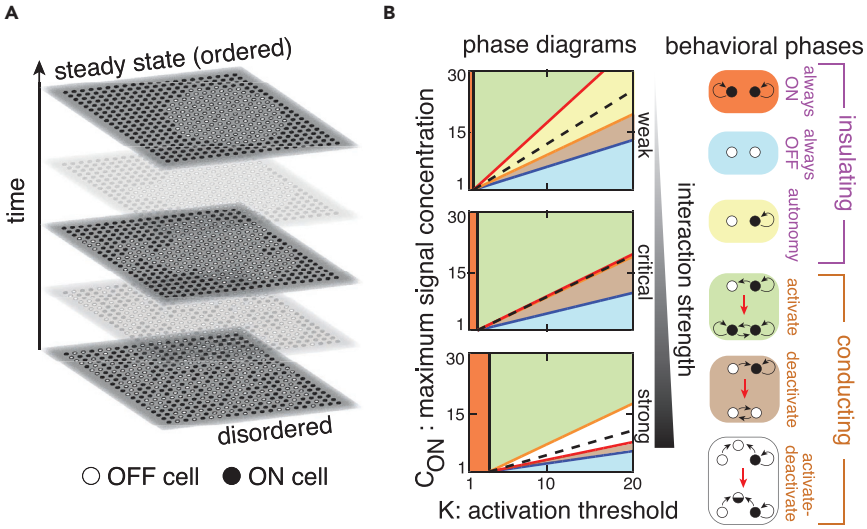

Figure 1. Secrete-and-Sense Cells Can Be Classified Into Distinct Behavioral Phases

(A) Snapshots of cellular automaton at different time points, in which an initially disordered cellular lattice becomes more ordered over time. White circle is an OFF-cell, and a black circle is an ON-cell.

(B) (Left column): Phase diagrams for a weak interaction (top panel; $f_N(a_o) < 1$), a critical interaction (middle panel; $f_N(a_o) = 1$), and a strong interaction (bottom panel; $f_N(a_o) > 1$), where the interaction strength is defined as $f_N(a_o) \equiv \sum_{i,j} \frac{e^{R-r_{ij}}}{r_{ij}} \sinh(R)$. (Right column): Different colors denote distinct behavioral phases.

See also Table S1.

communication between two cells, cell-i and cell-j, is quantified by an "interaction term" for that pair, $f(r_{ij}) \equiv \frac{e^{R-r_{ij}}}{r_{ij}} \sinh(R)$ (where r_{ij} is the distance between the centers of cell-i and cell-j and R is both cells' radius). This term is directly proportional to the concentration of the signaling molecule on cell-i that is due to cell-j, and vice versa. We then quantify the competition between the self- and neighbor communication among the N cells with the "interaction strength," $f_N(a_o) \equiv \sum_{i,j} \frac{e^{R-r_{ij}}}{r_{ij}} \sinh(R)$, which is the sum of the interaction terms of all cell pairs. It is a function only of the cells' radius R and the lattice spacing a_0. The latter is because all distances between the cells are determined by specifying the lattice spacing. The interaction strength $f_N(a_o)$ measures how much each cell captures the signals from all the other cells (see Supplemental Information section S1) (Maire and Youk, 2015b). For a given interaction strength, the activation threshold K and the C_{ON} determine the cells' behavioral phase. The values of K, C_{ON}, and f_N are held fixed, and thus the cells' behavioral phase also remains unchanged over time. We categorize a behavioral phase as either an "insulating phase"—in which no cell can turn on/off the other cells due to dominant self-communication—or a "conducting phase"—in which cells can turn on/off the others due to dominant neighbor communication (Figure 1B). Regardless of the interaction strength, cells can operate in two conducting phases: (1) "activate phase," in which neighboring ON-cells can turn on an OFF-cell, and (2) "deactivate phase," in which neighboring OFF-cells can turn off an ON-cell. In addition, when the interaction is weak [i.e., $f_N(a_0) < 1$], cells can operate in an "autonomy phase," which is an insulating phase whereby a cell can stay ON/OFF regardless of the other cells' states. On the other hand, when the interaction is strong [i.e., $f_N(a_0) > 1$], cells can operate in an "activate-deactivate phase," which is a conducting phase whereby the cells can both activate and deactivate the others depending on their relative locations.

Grouping Multiple Spatial Configurations Into One Macrostate Based on Their Common Spatial Index *I* and Fraction *p* of Cells that Are ON

We now present our framework's central ingredient. Let us define two "macrostate" variables: (1) the fraction p of cells that are ON (equivalent to the average gene-expression level) and (2) a "spatial index" I that we define as

$$I = \frac{N}{\sum_{i,j\neq i} f(r_{ij})} \frac{\sum_{i,j\neq i} f(r_{ij})(X_i - \langle X\rangle)(X_j - \langle X\rangle)}{\sum_i (X_i - \langle X\rangle)^2}, \qquad \text{(Equation 1)}$$

where X_i is +1 (−1) for an ON (OFF)-cell and $\langle X\rangle = \frac{1}{N}\sum_i X_i$ is the average over all the cells. The spatial index I, in fact, belongs to a widely used class of statistical metrics called Moran's I (Moran, 1950). Moran's I is frequently used for spatial analysis in diverse fields, including geographical analysis (Getis and Ord, 1992), ecology (Legendre, 1993), and econometrics (Anselin, 2008). Our spatial index I measures a spatial autocorrelation among the cells by weighing each cell pair by that pair's interaction term $f(r_{ij})$ (Maire and Youk, 2015b). Thus, roughly speaking, the spatial index measures the average correlation between the states of any two cells by assigning a higher weight to those cell pairs that communicate more with each other (i.e., more signal is shared between them). By construction, $-1 \leq I \leq 1$ and $0 \leq p \leq 1$. When $I = 0$, ON- and OFF-cells are randomly distributed across the lattice, yielding maximally disordered lattices (Figure 2A, top row, and Figure S1). When $|I|$ is large, the cells are more spatially ordered and the lattice consists of large contiguous clusters of ON/OFF-cells (Figure 2A, bottom row, and Figure S1). For $I > 0$, cells of the same ON/OFF-state tend to cluster together, whereas for $I < 0$, cells of the same ON/OFF-state tend to avoid each other (Figure S1). As we will see below, we can focus on lattices with a positive spatial index for our purpose. For positive values of I, a key feature that the value of the spatial index tells us is whether the lattice consists of one large, contiguous island of ON/OFF-cells (when I is close to one; Figure 2A, bottom row) or of many fragmented small islands of ON/OFF-cells (when I is close to zero; Figure 2A, top row). Our central idea is to group cellular lattices that have the same (p, I) into a single ensemble (examples in Figure 2A). We then view this ensemble as a particle that moves in an abstract space whose position at time t is ($p(t)$, $I(t)$). We call this abstract space a "phase space" because each point (p, I) in this space represents an ensemble of all possible spatial configurations that have the same value of p and the same value of I. The procedure of grouping spatial configurations based on their (p, I) is akin to a situation in physics in which many microstates (e.g., the positions and momenta of all particles) are grouped into a single macrostate (e.g., pressure or temperature). Thus, we will call each lattice configuration a "microstate," and the ensemble of these microstates represented by a given (p, I), a "macrostate" (Figure 2A).

Cellular Lattice Is Represented by a Particle Whose Position (p, I) and Trajectory Depend on the Behavioral Phase

By randomly choosing thousands of microstates that all belong to the same disordered macrostate ($p = p_{initial}$, $I \approx 0$) and then running the cellular automaton on each of these microstates, we observed how the lattices evolved out of disorder. Specifically, we obtained a distribution of their trajectories, and thus also a distribution of their final positions ($p = p_{final}$, $I = I_{final}$), for every value of $p_{initial}$ in each behavioral phase (Figures 2B and S3). The fact that we obtained, for a fixed value of $p_{initial}$, a distribution of values for p_{final} (Figure 2B, top row) and a distribution of trajectories (Figure 2B, bottom row) instead of a single trajectory, indicates that the particle moves stochastically in the p-I space. This stochasticity arises from the cellular automaton operating on individual cell's state X_i, a microstate variable, at each time step rather than operating on the macrostate variables, p and I. Also, since, at the macrostate level, we are ignorant of the exact microstate that the cellular automaton is operating on, the macrostate-level description of the particle's motion, once we deduce it, would have to be a stochastic description. We found several promising signs that an analytical, macrostate-level description is possible. First, we observed that particles that started at the same position ($p_{initial}$, 0), for the most part, remained close to each other in subsequent times, leading to tightly bundled trajectories in the p-I space despite the stochasticity (Figure 2B, bottom row). Furthermore, we observed other features that were shared by all the trajectories for each behavioral phase. Specifically, in the activate phase, we observed that if the $p_{initial}$ was above a certain threshold value (red vertical line in Figure 2B, top left panel), then almost all cells were turned on, whereas if it was below the threshold value, then the activation was minimal owing to the cellular automaton not starting with enough ON-cells. In the deactivate phase, we observed that if the $p_{initial}$ was below a certain threshold value (red vertical line in Figure 2B, top middle panel), then almost all cells turned off, whereas if it was above the threshold, then the deactivation of ON-cells was minimal owing to the cellular automaton not starting with enough OFF-cells. Finally, in the activate-deactivate phase, we

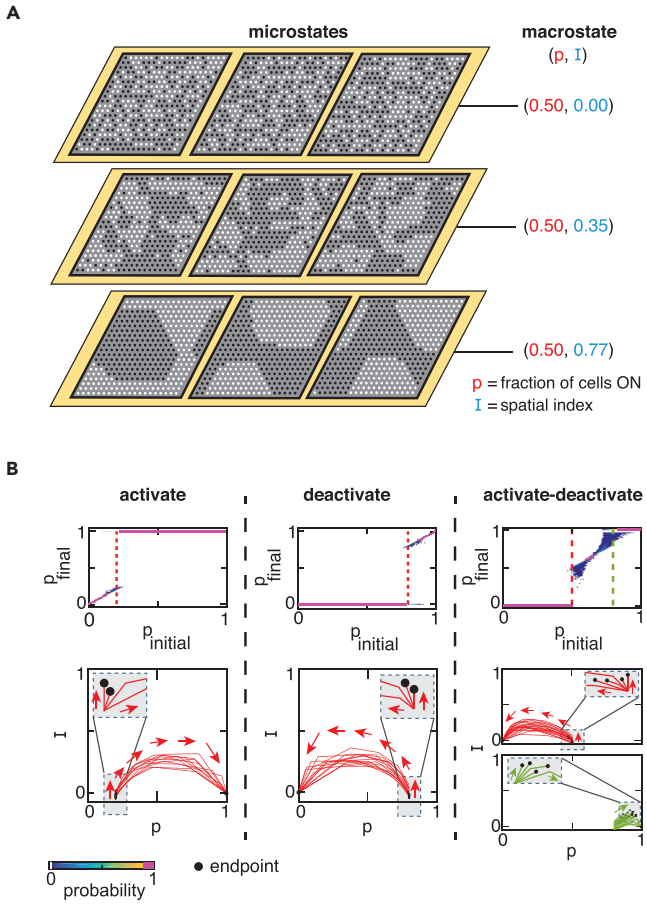

Figure 2. Spatial Configurations of Secrete-and-Sense Cells (microstates) Can Be Grouped into Macrostates

(A) Examples of microstates that have the same fraction of cells being ON (denoted *p*) and spatial index *I* grouped into a single macrostate, denoted by (*p, I*). For each macrostate (*p, I*), three microstates are shown as examples.

(B) (Top row): Probability density maps showing the particle's final value of *p* (denoted p_{final}) for each initial value of *p* (denoted $p_{initial}$) in the activate phase, deactivate phase, and activate-deactivate phase. Color code for the probability density is shown in the color bar at the bottom. The red dashed line in the activate phase (left panel) and the green dashed line in the activate-deactivate phase (right panel) approximate the lowest value of $p_{initial}$ that is required to turn on every cell (i.e., reach $p_{final} = 1$). The red dashed line in the deactivate phase (middle panel) and in the activate-deactivate phase approximates the highest value of $p_{initial}$ required to turn off every cell (i.e., reach $p_{final} = 0$). (Bottom row): Trajectories (red and green curves) in *p*-*I* space (called "phase space") in the activate phase (left panel), deactivate phase (middle panel), and activate-deactivate phase (right panel). Gray insets show zoomed-in views of some trajectories. Black dots denote the trajectories' endpoints.

See also Figure S1.

observed a threshold value for activation (green vertical line in Figure 2B, top right panel) and a threshold value for deactivation (red vertical line in Figure 2B, top right panel). Between these two thresholds, a particle stops with a value of *p* that is either only slightly higher (activation) or slightly lower (deactivation) than the value that it started with (giving rise to a slanted "bow tie" shape in Figure 2B, top right panel). We also observed common features in the shapes of the trajectories themselves in the *p*-*I* space. Specifically, we observed that in every trajectory, the *I* initially increased before plateauing at some value, whereas the *p* either monotonically increased or decreased over time (Figure 2B, bottom row). Then, one of two events occurred in all trajectories: either (A) the particle stopped, and thus the cellular automaton terminated, with the final value of *p* (i.e., p_{final}) between zero and one (see black dots that mark the trajectories' endpoints in Figure 2B, bottom row) or (B) the particle kept increasing or decreasing its *p* until it reached and stopped at either $p = 1$ (all cells ON) or $p = 0$ (all cells OFF), and as it did so, its spatial index abruptly dropped to zero (e.g., most of the red trajectories in Figure 2B). Observation (A) corresponds to a situation in which the cells form an ordered spatial configuration that, being a steady state of the cellular

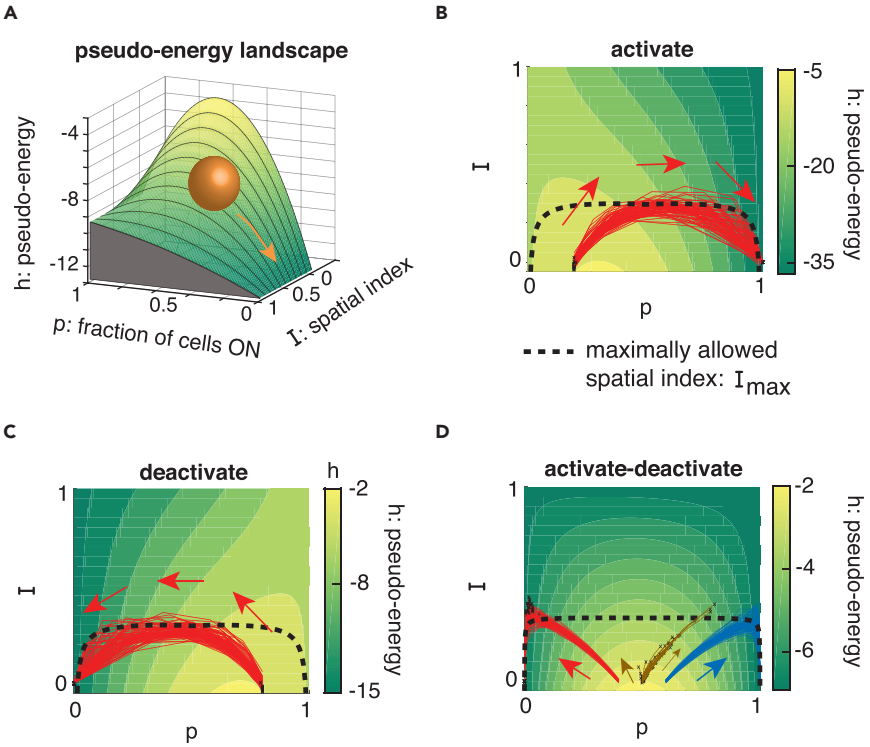

Figure 3. A Cellular Lattice Acts as a Particle that Rolls Down on and Adheres to a Pseudo-Energy Landscape

(A) Pseudo-energy landscape with a height defined by the pseudo-energy function $h(p, I)$. Orange ball is a particle that represents a cellular lattice. The landscape is defined over a position (p, I). A pseudo-energy landscape for (B) activate phase, (C) deactivate phase, and (D) activate-deactivate phase.

(B–D) Trajectories of the same color start from the same position in each landscape. Black curves show maximally allowed value of the spatial index I [i.e., function defined as $I_{max}(p)$ in the main text; see Supplemental Information section S4]. See also Figures S2 and S3.

automaton, remains unchanged indefinitely. This situation arose most notably but not exclusively in the activate-deactivate phase. Observation (B) corresponds to a situation in which all cells either turn on or off.

To explain observation (B), we first rewrite Equation 1 as (Supplemental Information section S2)

$$I(p) = \frac{\Theta - (2p-1)^2 f_N(a_O)}{4p(1-p) f_N(a_O)}, \qquad \text{(Equation 2)}$$

where $\Theta = \frac{1}{N}\sum_{i,j\neq i} f(r_{ij}) X_i X_j$. Note that the p and the spatial index I depend on each other. And since Equation 2 enables us to deduce the Θ if we know the I, and vice versa, we have the option of considering (p, Θ) to be a macrostate instead of (p, I). The main disadvantage of this is that the Θ, unlike the spatial index, is not normalized. This makes it difficult to compare the values of Θ for lattices with different values of p. Thus we will work with (p, I) instead of (p, Θ). From a mean-field approximation, in which we calculate the average amount of signal sensed by each cell (Figure S2 and Supplemental Information section S3), we deduced that the particle's spatial index has an upper bound for each value of p. We denote this p-dependent maximal value of I by a function $I_{max}(p)$ (dashed black curves in Figure 3). The function $I_{max}(p)$ sharply drops to zero as p nears zero or one. Accordingly, as the particle's p nears zero or one, its spatial index should sharply decrease to zero in accordance with observation (B) (Figures 3B–3D). This makes sense because the spatial index is a measure of whether or not the lattice consists of a large, contiguous island of ON/OFF-cells. As the spatial index approaches zero, the lattice becomes populated with more fragments of smaller islands of ON/OFF-cells. When the p is near zero (one), as is the case when only one cell is ON (OFF), then no clusters

of ON-cells (OFF-cells) are possible since there is only one ON-cell (OFF-cell). Owing to this and from a rigorous calculation of how the I changes as the p approaches zero or one (Supplemental Information section S2), we find that the spatial index is indeed zero when the p is either zero or one. To fully explain the particle trajectories along with observations (A) and (B), we next sought an equation of motion for the particles.

Cellular Lattice Acts as a Particle that Rolls Down on and Adheres to a Pseudo-Energy Landscape

We conjectured that if a cellular lattice indeed moves like a particle, then there may be a "landscape" on which the particle rolls down. To explore this idea, we consider a function h that we call a "pseudo-energy" and define it as $h \equiv -\sum_i X_i(Y_i - K)/N$, where Y_i is the signal concentration on cell-i. In fact, we can rewrite h entirely in terms of the macrostate variables, p and I (Supplemental Information section S4). Plotting $h(p, I)$ yields a three-dimensional landscape that we call a "pseudo-energy landscape" (Figure 3A). Its shape depends on the cells' behavioral phase (Figures 3B–3D). Importantly, by plotting the trajectories on top of their respective landscapes, we observed that every particle's pseudo-energy (i.e., value of h) monotonically decreased over time until the particle stopped. We could also rigorously prove this (Supplemental Information section S4). The fact that the pseudo-energy is a decreasing function of the spatial index explains why trajectories in general tend toward increasing values of the spatial index (Figures 3B–3D).

To see, at the microstate level, why the cells' states become more spatially correlated over time, we rewrite the h as

$$h = -\alpha \sum_{i,j \neq i} f(r_{ij}) X_i X_j - B \sum_i X_i - N\alpha, \qquad \text{(Equation 3)}$$

where $\alpha \equiv (C_{ON} - 1)/(2N)$ and B is a "signal field" defined as $\alpha\,(1 + f_N(a_O)) - K/N$. Equation 3 is strikingly similar to the Hamiltonians of the Hopfield network (Hopfield, 1982) and magnetic spins with long-range interactions (Kirkpatrick and Sherrington, 1975; Tchernyshyov and Chern, 2011). Note that since $\alpha f(r_{ij}) > 0$ and the particle's pseudo-energy keeps decreasing over time before the particle stops, the cells must "align" their states with each other rather than "anti-align" (i.e., the pseudo-energy favors the pairing of two ON-cells rather than pairing of an ON-cell with an OFF-cell). In magnetic spin systems, this would be analogous to a ferromagnetic interaction. As in physical systems, we can view the signal field B as a macroscopic knob that we can tune to change the shape of the pseudo-energy landscape for a given cellular lattice. From the phase diagrams (Figure 1B), we can deduce that $B > 0$ in the activate phase; that $B < 0$ in the deactivate phase; and that B can be positive, negative, or zero in the activate-deactivate phase (depending on K and C_{ON}) (Figure S3). Intuitively, increasing the value of Θ, and thus the value of I (by Equation 2), corresponds to the formation of larger clusters of ON-cells and OFF-cells, which would in turn decrease the pseudo-energy because the first term in Equation 3 equals $-\alpha N\Theta$. Despite these similarities, we emphasize that the cellular lattice is not the same as an Ising spin system. For one, there is no real Hamiltonian in our framework that, for instance, gives rise to a Boltzmann distribution. Importantly, we have not used any quantities from physics in our framework, despite some similar properties shared by the framework presented here and those of statistical physics. In the Discussion section, we will elaborate further on these similarities and differences.

Gradient of the Pseudo-Energy and the Trapping Probability $P_{eq}(p, I)$ Completely Specify the Particle's Motion

To deduce how exactly the shape of the pseudo-energy landscape determines the particle's motion, we compared the gradient field of the pseudo-energy $-\nabla h(p, I)$ (arrows in Figures 4A–4D) with the particle trajectories produced by the cellular automaton (red curves in Figures 4A–4D). We discovered that the particles closely follow the streamlines that are dictated by the gradient field. From this and the aforementioned observation that the particles move stochastically, we conjectured that the particles may follow Langevin-type dynamics in which the particle drifts (rolls) down the pseudo-energy landscape due to the gradient field and diffuses due to a noise term. We then proposed a phenomenological equation of motion for the particle,

$$\big(\Delta p(t),\ \Delta I(t)\big) = -\nabla h\big(p(t), I(t)\big) \cdot \delta + \Big(\eta_p(t), \eta_I(t)\Big) \qquad \text{(Equation 4)}$$

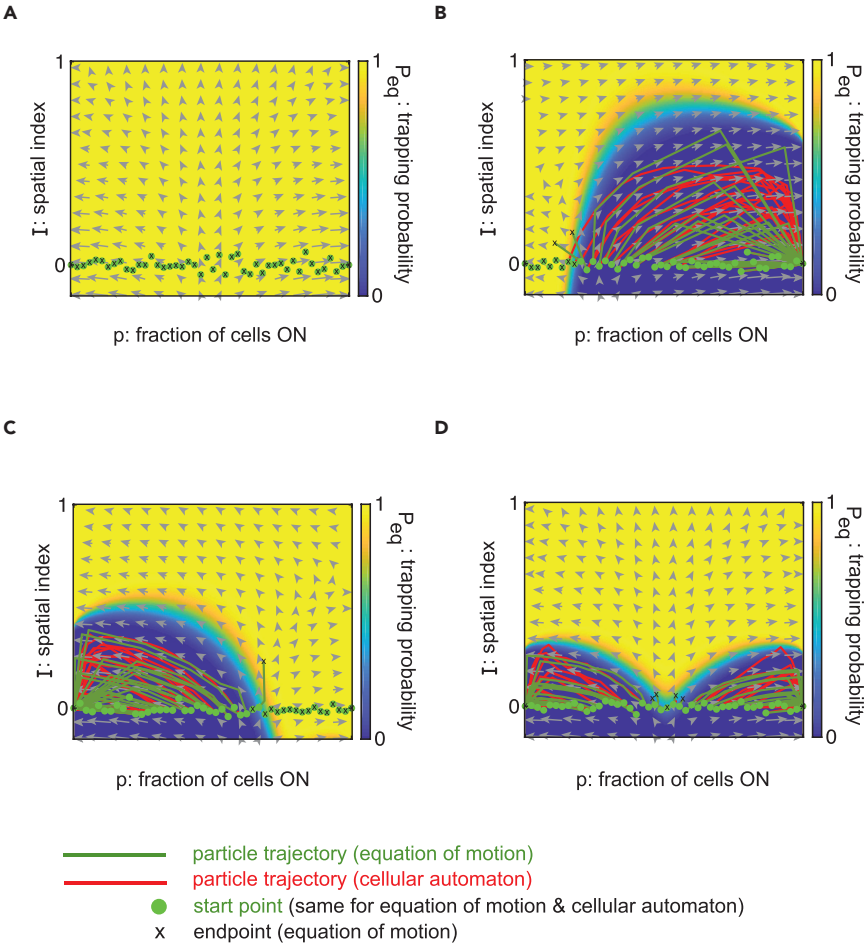

Figure 4. Gradient Field of the Pseudo-Energy, $-\nabla h(p, I)$, and the Trapping Probability, $P_{eq}(p, I)$, Completely Specify the Particle's Trajectory

(A–D) Each gray arrow represents the negative gradient of the pseudo-energy, $-\nabla h(p, I)$, at each position (p, I). Longer arrows indicate gradients of larger magnitudes. Heat maps show the magnitude of the trapping probability P_{eq} at each location (Supplemental Information section S5). Red trajectories are exact particle trajectories from the cellular automaton. Green trajectories are particle trajectories produced by Monte Carlo simulations that are dictated by the equation of motion (Equation 4) and the trapping probability. The green dots represent the starting points of the trajectories (same for the trajectories produced by the cellular automaton and the equation of motion), and the black crosses represent the endpoints of the green trajectories. (A) Autonomy phase, (B) activate phase, (C) deactivate phase, and (D) activate-deactivate phase.

See also Figures S4–S7.

Here $\Delta p(t)$ and $\Delta I(t)$ are changes in p and I, respectively, between time steps t and $t + 1$; δ is a constant factor that scales the gradient to account for the discreteness of time in the cellular automaton; and η_p and η_I are Gaussian noise terms that represent our ignorance of the microstates with a mean of zero and standard deviations of σ_p and σ_I, respectively. We determined δ, σ_p, and σ_I by calculating the mean and the variance of Δp, which in turn are set by the distribution of the signal concentrations that each cell senses for a given (p, I) (Supplemental Information sections S5-S6). Although the pseudo-energy determines the direction and the magnitude of changes in p and I, it does not predict where a particle stops on the landscape. As we noted earlier [observation (A)], the particle can stop before its value of p reaches zero or one. This corresponds to stopping at inclined regions of the pseudo-energy landscape. For this reason, we consider the landscape to be "adhesive," such that the particle can stop moving on its inclined regions. The gradient of the pseudo-energy is non-zero at such inclined locations, but the particle stops because it has adhered to the landscape at that location. Such particle adhesions occur frequently for the activate-deactivate phase and in the autonomy phase (e.g., termination points of the brown trajectories in Figure 3D). Crucially,

the particle halts in a stochastic manner, meaning that for two particles that pass through the same location (p, I), one may get stuck there, whereas the other does not. This is because each macrostate (p, I) can include microstates that are steady states of the cellular automaton and microstates that are not. We need a probabilistic description of how likely it is that a particle at a given location halts since we do not know which microstate is represented by the moving particle when we run a Monte Carlo simulation of Equation 4. To obtain a stochastic description, we used a mean-field approach to estimate, for a given macrostate (p, I), the fraction of microstates in it that are steady states of the cellular automaton (Supplemental Information section S5). We call this fraction, which is between zero and one, the "trapping probability" and denote it by $P_{eq}(p, I)$. It is the probability that a particle at location (p, I) corresponds to a steady state of the cellular automaton and thus halts there. Roughly speaking, the trapping probability $P_{eq}(p, I)$ represents the "adhesiveness" of the landscape that we discussed earlier. To produce particle trajectories, we ran a Monte Carlo simulation that combines the phenomenological equation of motion (Equation 4) and the condition that the particle halts at location (p, I) with a probability $P_{eq}(p, I)$ (Supplemental Information section S6). We found that the particle trajectories obtained from these Monte Carlo simulations (green curves in Figures 4A–4D) recapitulated, for a wide range of parameters, the main qualitative features of the particle trajectories that the cellular automaton produces (red curves in Figures 4A–4D), including the general regions where the particles get stuck, despite some deficiencies (Figures S4–S7). We will discuss the limitations of this approach in the Discussion section.

Stochastic Sensing Can Yield Spatial Configurations that Are More Ordered than Those Formed without Noise

Having shown where the particle gets stuck on the pseudo-energy landscape, a natural question is how stably the particle sticks at each location. Biological noise is a sensible context to address this question. To address this question and as a proof of principle for demonstrating how to include stochastic gene expression in our framework (Raj and Van Oudenaarden, 2008; Sagués et al., 2007; García-Ojalvo, 2011; Tkačik and Walczak, 2011; Sanchez and Golding, 2013; Xu et al., 2016; Friedman et al., 2006), we modified the deterministic cellular automaton that we have been using thus far to include stochastic sensing. Specifically, for each cell and at each time step of the cellular automaton, we now pick a new value for the activation threshold, $K + \delta K$. Here, K is the same value for every cell at all times and δK is a Gaussian noise term with a mean of zero and a variance of α^2 (Figure 5A and Supplemental Information section S7). We then define a "noise strength," $\xi = \alpha/K$, that helps us determine how much noise is required to liberate an adhered particle and cause a moving particle to significantly deviate from the path that it would have taken if there were no noise. Intuitively, we would expect such deviations to occur if the noise δK is sufficiently large, such that either an ON-cell, on which the average signal concentration $\langle Y_{ON} \rangle$ is larger than the activation threshold without the noise, K, would turn off due to the noise increasing the activation threshold so that it becomes larger than $\langle Y_{ON} \rangle$, or an OFF-cell, on which the average signal concentration $\langle Y_{OFF} \rangle$ is smaller than K, would turn on due to the noise decreasing the activation threshold so that it becomes smaller than $\langle Y_{OFF} \rangle$. Mathematically, this means that we would expect the minimum noise strength ξ_{min} required to significantly perturb the particle trajectories to be $\min(|\langle Y_{ON} \rangle - K|, |\langle Y_{OFF} \rangle - K|)/(K\sqrt{N})$ (Supplemental Information section S7 and Figure S8). Indeed, we found that a very weak noise (i.e., $\xi \ll \xi_{min}$) cannot detach an adhered particle from the landscape (Figure 5B, left column), whereas a very strong noise (i.e., $\xi \gg \xi_{min}$) can detach an adhered particle and thereby cause the particle to roll down the landscape further. After being detached, the particle further changes its p, decreases its pseudo-energy, and increases its spatial index until its p reaches either zero or one (Figure 5B, right column). Moreover, we found that a moderate noise (i.e., $\xi \sim \xi_{min}$) can liberate the adhered particle and push it further down the landscape, beyond the previously allowed region of the landscape (i.e., beyond the region bounded by $I_{max}(p)$ [black curve in Figure 5C]), until it adheres to the landscape again, but now with a higher spatial index than before and with an intermediate value of p I (i.e., $0 < p < 1$) (Figures 5C and S9). Intriguingly, when there is a moderate noise in the activate-deactivate phase, we observed that some of the trapped particles' p, I, and h very slowly changed over time, allowing the particles to remain stuck with an intermediate value of p over hundreds but not thousands of time steps (Figure 5D). As a follow-up study, it would be interesting to examine if this phenomenon is similar to the glass-type dynamics seen in physics.

DISCUSSION

Here we have uncovered a visual landscape for a ubiquitous form of cellular communication, called secreting and sensing, and showed that it underlies how simple secrete-and-sense cells' gene expressions become more spatially correlated over time in the absence of any pre-existing morphogens. Instead of focusing on how specific spatial patterns such as stripes and islands emerge, we focused on the overall

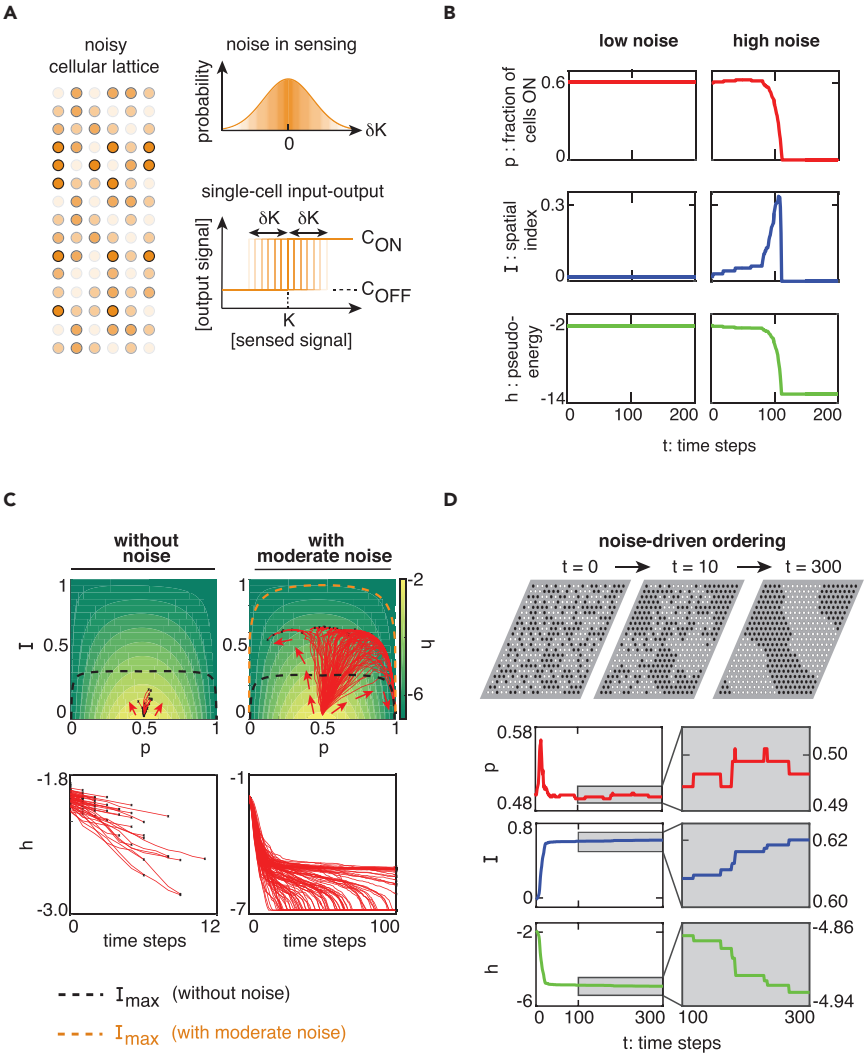

Figure 5. Stochastic Sensing Can Yield Spatial Configurations That Are More Ordered than Those Formed without Noise

(A) (Left column) Schematics of secrete-and-sense cells with noisy sensing. Each cell (circle) is colored by a different shade of orange, with a darker shade representing less noise. (Top right panel) Noise in activation threshold K, denoted δK, is normally distributed with a zero mean and a variance α^2. (Bottom right panel) Range of activation thresholds $K + \delta K$ for each cell.

(B) Examples of changing fraction p of cells that are ON, spatial index I, and pseudo-energy h for low noise (left column; $\xi < \xi_{min}$) and high noise (right column; $\xi > \xi_{min}$) in the activate-deactivate phase. $\xi = \alpha/K$ is the noise strength and ξ_{min} is the minimum noise strength required to detach an adhered particle (Supplemental Information section S7). Both the low noise and the high noise scenarios begin with a spatial configuration that is a steady state of the deterministic cellular automaton.

(C) Particle trajectories (red curves), in activate-deactivate phase, for a deterministic cellular automaton (left column) and cellular automaton with a moderate noise (i.e., $\xi < \xi_{min}$) in sensing (right column). All trajectories start at ($p = 0.5$, $I \approx 0$). Black dots show endpoints of trajectories. Calculated maximum I as a function of p when no noise is absent (black curve) and when a moderate noise is present (orange curve) are shown (also see Supplemental Information section S3).

(D) (Top panel) Snapshots at different times of cellular lattice becoming more ordered due to noise in sensing in the activate-deactivate phase. Black circles are ON-cells, and white circles are OFF-cells. (Bottom panel): Fraction p of cells that are ON (red curve), spatial index I (blue curve), and pseudo-energy h (green curve) over time for the pattern formation shown in the top panel. Zoomed-in views (gray boxes) show slowly changing p (red curve), I (blue curve), and h (green curve) that occur while the cellular lattice is in a highly ordered metastable configuration (shown at $t = 300$ in the top panel).

See also Figures S8–S10.

spatial order, a statistical measure of cell-cell coordination of gene expressions that we called spatial index. This macrostate-level description has the advantage of making exhaustive, numerical simulations that are typically used for these systems unnecessary but has the disadvantage of being ignorant of the specific spatial patterns that form. The spatial index, however, still allows us to discern what kinds of spatial patterns are formed because fixing its value restricts the spatial patterns that are possible (Figure 2A). Toward showing that our approach may be adapted to other types of cell-cell communication, we show, in the Supplemental Information, how to extend our framework to lattices with multiple cell types and signal types (Supplemental Information section S8 and Figure S10). These include paracrine signaling, in which one cell secretes a signal without sensing it, whereas another type of cell senses without secreting that signal (Doğaner et al., 2016). Despite its wide applicability, there are instances where the current framework would not apply. We now turn to discussing these situations before concluding with a discussion on how our framework is distinct from that of physics and how one can apply our model to experiments.

Our modeling framework for secrete-and-sense cells with a bistable (ON/OFF) gene expression relied on meeting two conditions: (1) every cell adjusting its ON/OFF-state within the same timescale and (2) the concentration of the signaling molecule on each cell reaching a steady state before the cell can switch its ON/OFF-state. The first condition sets the actual time that each discrete time step of the cellular automaton represents and is the reason that the cellular automaton simultaneously updated every cell's state. It is satisfied if the variability among cells in their response times to the signaling molecule (i.e., time taken by each cell to change between ON- and OFF-states) is smaller than the average response time of the cell. The second condition, which states that the typical response time of the cells is larger than the time that the signaling molecule takes to form a steady-state concentration, is satisfied in several biological processes. They include the aforementioned yeasts that secrete and sense the mating pheromone and the regenerating hair follicles in mice (Youk and Lim, 2014a; Chen et al., 2015; Rappaport and Barkai, 2012; Maire and Youk, 2015a). The condition is also satisfied by several quorum-sensing bacteria (e.g., ~20–30 s to establish a steady-state concentration) (Kaplan and Greenberg, 1985; Pearson et al., 1999). Despite these examples, a major aspect that we have neglected is that signaling molecules are often affected by processes other than diffusion such as active transporting of the molecules and clustering and endocytosis of receptors. Several studies of morphogen gradients in developing embryos, however, have shown that in many cases, one can use a simple diffusion alone to mathematically reproduce the creation dynamics of morphogen gradients even when there are other processes (Lander et al., 2002). Finally, aside from conditions (1) and (2), our model assumes that cells are arranged on a triangular lattice. Indeed, several systems, including the nuclei inside the early *Drosophila melanogaster* embryo, can be approximated as being arranged on a triangular lattice despite not satisfying both conditions (1) and (2) (Gregor et al., 2007) (see other examples in Table S1). For other regular lattices, one can modify the framework by changing the functional form of the interaction strength $f_N(a_o)$.

Another element in our framework whose validity requires a careful thought is the equation of motion (Equation 4). The equation of motion is a phenomenological equation that recapitulates the main qualitative features of the particle trajectories but does not reproduce the exact location of the particle at every time step of the cellular automaton (Figures 4A–4D). As an example, given any initial value of the fraction p of ON-cells, the equation of motion accurately predicts whether the p will increase, decrease, or stay the same (Figure S6). However, the trajectories produced by the equation of motion do not exactly match those produced by the cellular automaton. In particular, the trajectories produced by the equation of motion are least likely to match those of the cellular automaton at locations where the gradient vector of the pseudo-energy is perfectly horizontal (i.e., parallel to the p-axis) or vertical (i.e., parallel to the I-axis), and most likely to match when the gradient is at 45° with respect to both axes. Since the gradient is neither perfectly horizontal nor vertical (Figures 4A–4D) at most locations, the gradient of the pseudo-energy together with the trapping probability P_{eq} (p, I) gives a qualitatively accurate description of the particle's motion. We also found that the equation of motion gives a more accurate description of the particle trajectories for strong interactions [i.e., $f_N(a_0) > 1$] than weak interactions [i.e., $f_N(a_0) < 1$]. To see why this is, note that we used mean-field approximations, in which we assumed that ON- and OFF-cells are randomly distributed, to determine the values of σ_p, σ_I and δ in the equation of motion (Equation 4) (Supplemental Information section S6). This mean-field approximation breaks down if long-lived, large islands of ON- and OFF-cells form and slowly grow over time. Such islands indeed frequently form when the interaction is weak and lead to the cellular automaton producing higher values of the spatial index I than the equation of motion allows for (Figure S4). In contrast, when the interaction is strong, the particle typically moves

faster because the effect of changing the ON/OFF-state of a single cell propagates to the faraway cells. Thus the entire lattice of cells typically turns on or off in a few time steps without clearly forming local domains of ON/OFF-cells that grow over time (Figure S5). Hence the equation of motion is more suitable for strong interactions than for weak interactions. Finally, we note that another source of quantitative disagreements between the equation of motion and the cellular automaton lies in the fact that in computing the gradient of the pseudo-energy, the equation of motion assumes that p and I are continuous variables when in fact they are discrete quantities since the number of cells N is finite. This continuum approximation, however, is valid in the limit of the population size approaching infinity. This is because the spacing between two adjacent values of p is 1/N and the spacing between two adjacent values of I for a fixed value of p scales as 1/N (when p is neither zero nor one; note that there is only one value for I when p is zero or one).

In this article, we have shown that it is possible build a physics-type framework for complex multicellular systems that are governed by chemical signals, gene-regulatory networks, and multiple cells. Many such systems are currently only treated by exhaustive, numerical simulations and lack analytical frameworks of the type that we presented here. This situation has risen because the established metrics from physics, such as energy and momentum, are ill-suited for describing gene expressions and chemical signals in multicellular systems. Researchers have used physics-type frameworks to explain many-body living systems such as birds that flock together (Vicsek et al., 1995) and tissues that are subject to mechanical forces (Graner and Glazier, 1992), whereas multicellular systems of the type that we studied here, which are not governed by mechanical or electrical means, have been difficult to treat by directly applying existing concepts and quantities from physics. Despite the similarities in the approach that we have taken and that of statistical mechanics, our framework should not be interpreted in terms of existing quantities from physics because our model does not use any existing quantities of physics such as energy, force, momentum, or temperature. For example, the pseudo-energy (Equation 3) only mathematically takes the same form as the long-ranged Ising Hamiltonian. However, the particle does not follow the equations of Hamiltonian mechanics. As another example, the concepts of detailed balance and thermal equilibrium do not apply to the particle that is stuck on the pseudo-energy landscape. In other words, there is no state in which the macroscopic variables remain constant, whereas the cellular lattice dynamically transitions between microstates of the same macrostate. The notions of entropy and temperature also do not have straightforward definitions in our system. One can count the total number of microstates for a given (p, I) or the number of steady-state microstates for a given (K, C_{ON}) (Maire and Youk, 2015b), but neither would be a thermodynamic entropy. In light of these considerations, it would be interesting to explore, in a future work, if the quantities in our framework can be derived from the quantities of physics.

Experimentally, one can measure the two macrostate variables, p and I, in microscopic images [e.g., by tagging fluorescent protein(s) to the output gene(s)]. One may also use the tools of optogenetics to engineer the cells so that shining light on a single cell would cause the cell to secrete a signaling molecule or switch between the ON- and OFF-state (Guglielmi et al., 2016). One can then use light to sculpt a pattern of secreting ON-cells at the beginning of an experiment, in effect initializing the values of p and I, and then observe how the ON- and OFF-states change by recording over time the fluorescence of each cell, which reports whether the cell is ON or OFF. Our model and its extensions may help in understanding such microscope-based time-lapse movies of secrete-and-sense cells that form spatial patterns. Along with studying how specific spatial patterns, such as stripes and islands, are generated, it is useful to focus on statistically describing how certain classes of spatial patterns arise without knowing the exact spatial patterns involved, as we have done here. This is because one often cannot measure all the parameters that are required for constructing detailed numerical models (e.g., gene-expression level of every cell in a tissue). In such situations, our framework and its extensions may help in predicting, based on a limited knowledge of the underlying gene-regulation scheme and an estimate of the system's initial spatial order, how the spatial configuration of the cells evolves over time without revealing the exact location, shape, and size of the resulting spatial pattern. We hope that our work, along with complementary approaches for studying spatial patterns (Cotterell et al., 2015; Surkova et al., 2009; Sokolowski et al., 2012; Tkačik et al., 2008; Hillenbrand et al., 2016; Erdmann et al., 2009; Fancher and Mugler, 2017; Thalmeier et al., 2016), will inform ongoing efforts to establish quantitative frameworks for multicellular gene regulations.

METHODS

All methods can be found in the accompanying Transparent Methods supplemental file.

SUPPLEMENTAL INFORMATION

Supplemental Information includes Transparent Methods, 10 figures, and one table and can be found with this article online at https://doi.org/10.1016/j.isci.2018.03.013.

ACKNOWLEDGMENTS

We thank Yaroslav Blanter, Louis Reese, Arjun Raj, and the members of the Youk group for insightful discussions and comments on the manuscript. H.Y. is supported by the European Research Council's Starting Grant (MultiCellSysBio, #677972), the Netherlands Organisation for Scientific Research (NWO) Vidi award (#680-47-544), and the NWO NanoFront program.

AUTHOR CONTRIBUTIONS

E.P.O., Y.D., and H.Y. designed the research. E.P.O. and Y.D. performed the research with guidance from H.Y. All authors wrote the manuscript.

DECLARATION OF INTERESTS

The authors declare no competing interests.

Received: January 6, 2018
Revised: February 18, 2018
Accepted: February 22, 2018
Published: April 27, 2018

REFERENCES

Anselin, L. (2008). Spatial Econometrics: Methods and Models (Springer Science and Business Media).

Antebi, Y.E., Reich-Zeliger, S., Hart, Y., Mayo, A., Eizenberg, I., Rimer, J., Putheti, P., Pe'er, D., and Friedman, N. (2013). Mapping differentiation under mixed culture conditions reveals a tunable continuum of t cell fates. PLoS Biol. *11*, e1001616.

Chen, C.C., Wang, L., Plikus, M.V., Jiang, T.X., Murray, P.J., Ramos, R., Guerrero-Juarez, C.F., Hughes, M.W., Lee, O.K., Shi, S., et al. (2015). Organ-level quorum sensing directs regeneration in hair stem cell populations. Cell *161*, 277–290.

Coppey, M., Berezhkovskii, A.M., Sealfon, S.C., and Shvartsman, S.Y. (2007). Time and length scales of autocrine signals in three dimensions. Biophys. J. *93*, 1917–1922.

Cotterell, J., Robert-Moreno, A., and Sharpe, J. (2015). A local, self-organizing reaction-diffusion model can explain somite patterning in embryos. Cell Syst. *1*, 257–269.

Cotterell, J., and Sharpe, J. (2010). An atlas of gene regulatory networks reveals multiple three-gene mechanisms for interpreting morphogen gradients. Mol. Syst. Biol. *6*, 1–14.

Danino, T., Mondragón-Palomino, O., Tsimring, L., and Hasty, J. (2010). A synchronized quorum of genetic clocks. Nature *463*, 326–330.

De Monte, S., d'Ovidio, F., Danø, S., and Sørensen, P.G. (2007). Dynamical quorum sensing: population density encoded in cellular dynamics. Proc. Natl. Acad. Sci. USA *104*, 18377–18381.

Doğaner, B.A., Yan, L.K.Q., and Youk, H. (2016). Autocrine signaling and quorum sensing: extreme ends of a common spectrum. Trends Cell Biol. *26*, 262–271.

Erdmann, T., Howard, M., and Ten Wolde, P.R. (2009). Role of spatial averaging in the precision of gene expression patterns. Phys. Rev. Lett. *103*, 258101.

Ermentrout, G.B., and Edelstein-Keshet, L. (1993). Cellular automata approaches to biological modeling. J. Theor. Biol. *160*, 97–133.

Fancher, S., and Mugler, A. (2017). Fundamental limits to collective concentration sensing in cell populations. Phys. Rev. Lett. *118*, 078101.

Friedman, N., Cai, L., and Xie, X.S. (2006). Linking stochastic dynamics to population distribution: an analytical framework of gene expression. Phys. Rev. Lett. *97*, 168302.

García-Ojalvo, J. (2011). Physical approaches to the dynamics of genetic circuits: a tutorial. Contemp. Phys. *52*, 439–464.

Getis, A., and Ord, J.K. (1992). The analysis of spatial association by use of distance statistics. Geogr. Anal. *24*, 189–206.

Graner, F., and Glazier, J. (1992). Simulation of biological cell sorting using a two-dimensional extended Potts model. Phys. Rev. Lett. *69*, 2013–2016.

Gregor, T., Fujimoto, K., Masaki, N., and Sawai, S. (2010). The onset of collective behavior in social amoebae. Science *328*, 1021–1025.

Gregor, T., Tank, D.W., Wieschaus, E.F., and Bialek, W. (2007). Probing the limits to positional information. Cell *130*, 153–164.

Guglielmi, G., Falk, H.J., and De Renzis, S. (2016). Optogenetic control of protein function: from intracellular processes to tissue morphogenesis. Trends Cell Biol. *26*, 864–874.

Hart, Y., Reich-Zeliger, S., Antebi, Y.E., Zaretsky, I., Mayo, A.E., Alon, U., and Friedman, N. (2014). Paradoxical signaling by a secreted molecule leads to homeostasis of cell levels. Cell *158*, 1022–1032.

Hillenbrand, P., Gerland, U., and Tkačik, G. (2016). Beyond the French flag model: Exploiting spatial and gene regulatory interactions for positional information. PLoS One *11*, e0163628.

Hopfield, J.J. (1982). Neural networks and physical systems with emergent collective computational abilities. Proc. Natl. Acad. Sci. USA *79*, 2554–2558.

Kamino, K., Kondo, Y., Nakajima, A., Honda-Kitahara, M., Kaneko, K., and Sawai, S. (2017). Fold-change detection and scale invariance of cell-cell signaling in social amoeba. Proc. Natl. Acad. Sci. USA *114*, E4149–E4157.

Kaplan, H.B., and Greenberg, E.P. (1985). Diffusion of autoinducer is involved in regulation of the *Vibrio fischeri* luminescence system. J. Bacteriol. *163*, 1210–1214.

Kirkpatrick, S., and Sherrington, D. (1975). Solvable model of a spin-glass. Phys. Rev. Lett. *35*, 1792–1796.

Lander, A.D., Nie, Q., and Wan, F.Y.M. (2002). Do morphogen gradients arise by diffusion? Dev. Cell *2*, 785–796.

Legendre, P. (1993). Spatial autocorrelation: trouble or new paradigm? Ecology *74*, 1659–1673.

Liu, C., Fu, X., Liu, L., Ren, X., Chau, C.K.L., Li, S., Xiang, L., Zeng, H., Chen, G., Tang, L.-H., et al.

(2011). Sequential establishment of stripe patterns in an expanding cell population. Science *334*, 238–241.

Maire, T., and Youk, H. (2015a). A collective path to regeneration. Cell *161*, 195–196.

Maire, T., and Youk, H. (2015b). Molecular-level tuning of cellular autonomy controls the collective behaviors of cell populations. Cell Syst. *1*, 349–360.

Mehta, P., Goyal, S., Long, T., Bassler, B.L., and Wingreen, N.S. (2009). Information processing and signal integration in bacterial quorum sensing. Mol. Syst. Biol. *5*, 1–11.

Moran, P.A.P. (1950). Notes on continuous stochastic phenomena. Biometrika *37*, 17–23.

Pai, A., Tanouchi, Y., and You, L. (2012). Optimality and robustness in quorum sensing (QS)-mediated regulation of a costly public good enzyme. Proc. Natl. Acad. Sci. USA *109*, 19810–19815.

Pearson, J.P., Van Delden, C., and Iglewski, B.H. (1999). Active efflux and diffusion are involved in transport of *Pseudomonas aeruginosa* cell-to-cell signals. J. Bacteriol. *181*, 1203–1210.

Raj, A., and Van Oudenaarden, A. (2008). Nature, nurture, or chance: stochastic gene expression and its consequences. Cell *135*, 216–226.

Rappaport, N., and Barkai, N. (2012). Disentangling signaling gradients generated by equivalent sources. J. Biol. Phys. *38*, 267–278.

Sagués, F., Sancho, J.M., and García-Ojalvo, J. (2007). Spatiotemporal order out of noise. Rev. Mod. Phys. *79*, 829–882.

Sanchez, A., and Golding, I. (2013). Genetic determinants and cellular constraints in noisy gene expression. Science *342*, 1188.

Sawai, S., Thomason, P.A., and Cox, E.C. (2005). An autoregulatory circuit for long-range self-organization in Dictyostelium cell populations. Nature *433*, 323–326.

Sgro, A.E., Schwab, D.J., Noorbakhsh, J., Mestler, T., Mehta, P., and Gregor, T. (2015). From intracellular signaling to population oscillations: bridging size- and time-scales in collective behavior. Mol. Syst. Biol. *11*, 779.

Shvartsman, S.Y., Wiley, H.S., and Deen, W.M. (2001). Spatial range of autocrine signaling: modeling and computational analysis. Biophys. J. *81*, 1854–1867.

Sokolowski, T.R., Erdmann, T., and Ten Wolde, P.R. (2012). Mutual repression enhances the steepness and precision of gene expression boundaries. PLoS Comp. Biol. *8*, e1002654.

Sporn, M.B., and Todaro, G.J. (1980). Autocrine secretion and malignant transformation of cells. N. Engl. J. Med. *303*, 878–880.

Surkova, S., Spirov, A.V., and Gursky, V.V. (2009). Canalization of gene expression and domain shifts in the *Drosophila* blastoderm by dynamical attractors. PLoS Comp. Biol. *5*, e1000303.

Tchernyshyov, O., and Chern, G.W. (2011). Spin-lattice coupling in frustrated antiferromagnets. In Introduction to Frustrated Magnetism, C. Lacroix, P. Mendels, and F. mila, eds. (Springer), pp. 269–291.

Thalmeier, D., Halatek, J., and Frey, E. (2016). Geometry-induced protein pattern formation. Proc. Natl. Acad. Sci. USA *113*, 548–553.

Tkačik, G., Gregor, T., and Bialek, W. (2008). The role of input noise in transcriptional regulation. PLoS One *3*, e2774.

Tkačik, G., and Walczak, A.M. (2011). Information transmission in genetic regulatory networks: a review. J. Phys. Condens. Matter *23*, 153102.

Umeda, T., and Inouye, K. (2004). Cell sorting by differential cell motility: a model for pattern formation in Dictyostelium. J. Theor. Biol. *226*, 215–224.

Vicsek, T., Czirók, A., Ben-Jacob, E., Cohen, I., and Shochet, O. (1995). Novel type of phase transition in a system of self-driven particles. Phys. Rev. Lett. *75*, 1226–1229.

Xu, H., Skinner, S.O., Sokac, A.M., and Golding, I. (2016). Stochastic kinetics of nascent RNA. Phy. Rev. Lett. *117*, 128101.

You, L., Cox, R.S., Weiss, R., and Arnold, F.H. (2004). Programmed population control by cell-cell communication and regulated killing. Nature *428*, 868–871.

Youk, H., and Lim, W.A. (2014a). Secreting and sensing the same molecule allows cells to achieve versatile social behaviors. Science *343*, 1242782.

Youk, H., and Lim, W.A. (2014b). Sending mixed messages for cell population control. Cell *158*, 973–975.

ISCI, Volume *2*

Supplemental Information

Statistical Dynamics of Spatial-Order Formation by Communicating Cells

Eduardo P. Olimpio, Yiteng Dang, and Hyun Youk

Supplemental Information

Supplemental Data Items

Biological System	a_0	R	λ	τ_{ss}	References (see caption)
Hair follicle regeneration	150μm	25-50μm*	1mm	<1 day	[1]
Drosophila melanogaster Bicoid-Hunchback	8.5μm	3.25μm	100 μm	90 min	[2]
Drosophila melanogaster ommatidia	17.5μm	8.75μm**	-†	-†	[3-6]
Drosophila melanogaster wing development	3μm	1.45μm	220μm	6-8 hours	[7-9]
Zebrafish embryogenesis Nodal activator	20μm	10μm	135μm	-†	[10]
Xenopus laevis growth factor	$20-30\mu$m	$10-15\mu$m	100μm***	5 min****	[11, 12]

Table S1: (Related to Figure 1) **Secrete-and-sense systems that are arranged on nearly triangular lattices that motivated our work.** a_0 is the approximate distance between the centers of the cells. R is the average radius of the cells. The signalling molecule has a characteristic diffusion length λ. τ_{ss} is the time needed to establish a steady state profile. *Notes:* *The radius, measured as the typical size of the hair follicle's base, was inferred from the images in the reference. **The structure is an extruded hexagon and cannot be approximated by a single radius. The reported value is half the distance between the centers of the ommatidia units. ***Assumed to be half the length of the gradient. **** τ_{ss} not reported in paper, but calculated from the estimate $\tau_{ss} \sim r^2/D$ where r is the typical length scale in the system and D is the diffusion constant (reported). † Quantity not known or not measured. - References in the table: [1] Chen et al. Cell (2015); [2] Gregor et al. Cell (2007); [3] Mikeladze-Dvali et al. Cell (2005); [4] Posnien et al. PLoS ONE (2012); [5] Tsachaki et al. Dev. Dynamics (2012); [6] Yang et al. Cell (2002); [7] Entchev et al. Cell (2000); [8] Lander et al. Dev. Cell (2002); [9] Teleman et al. Cell (2000); [10] Muller et al. Science (2012); [11] Green. Dev Dynamics (2002); [12] McDowell et al. Dev. Biol. (2001)

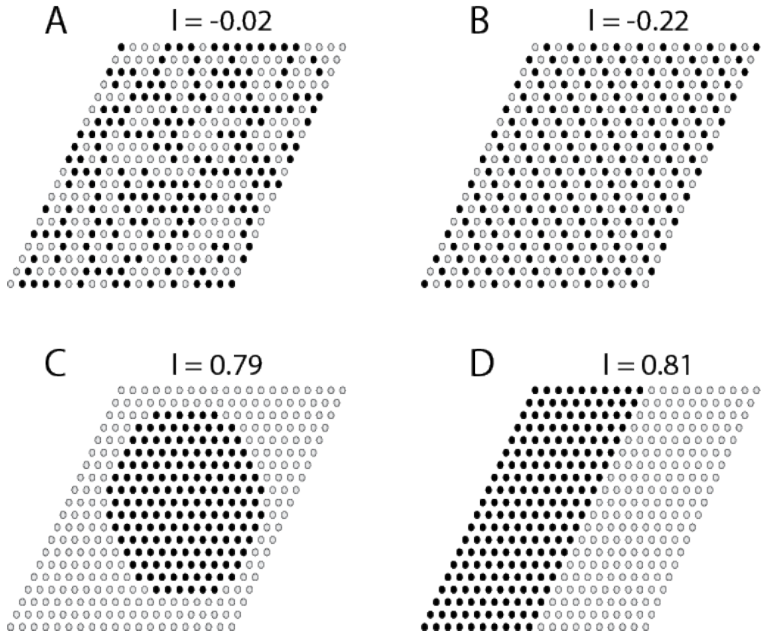

Figure S1: (Related to Figure 2) **Spatial index I.** For all the spatial configurations depicted here, we used $a_0 = 1.5$, $R = 0.2a_0$ and $N = 400$ cells (in a 20×20 grid). **A.** 200 ON-cells randomly arranged (near maximal disorder: $I \approx 0$. **B.** Chessboard-like configuration with 200 ON-cells. **C.** Circular island of 163 ON-cells. **D.** Stripe of 200 ON-cells.

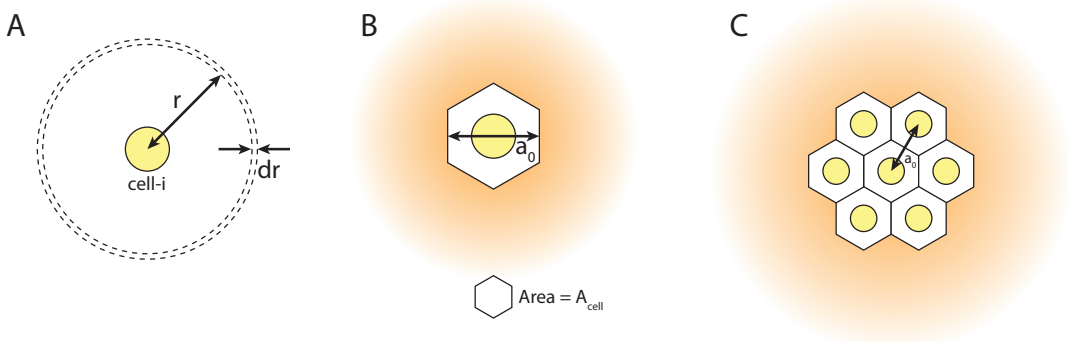

Figure S2: (Related to Figure 3) **Schematics for computing the number density for approximating the interaction strength for an arbitrary distribution of cells. A.** The number density is given by the number of cells inside a thin circle centered at cell-i with radius r and width dr. **B.** We approximate the interaction strength by considering the cells to be continuously distributed in space, resulting in equation S37. **C.** A better approximation for the interaction strength: Treating the nearest neighbours of a cell exactly while considering the rest of the cells to be continuously distributed throughout space, resulting in equation S43.

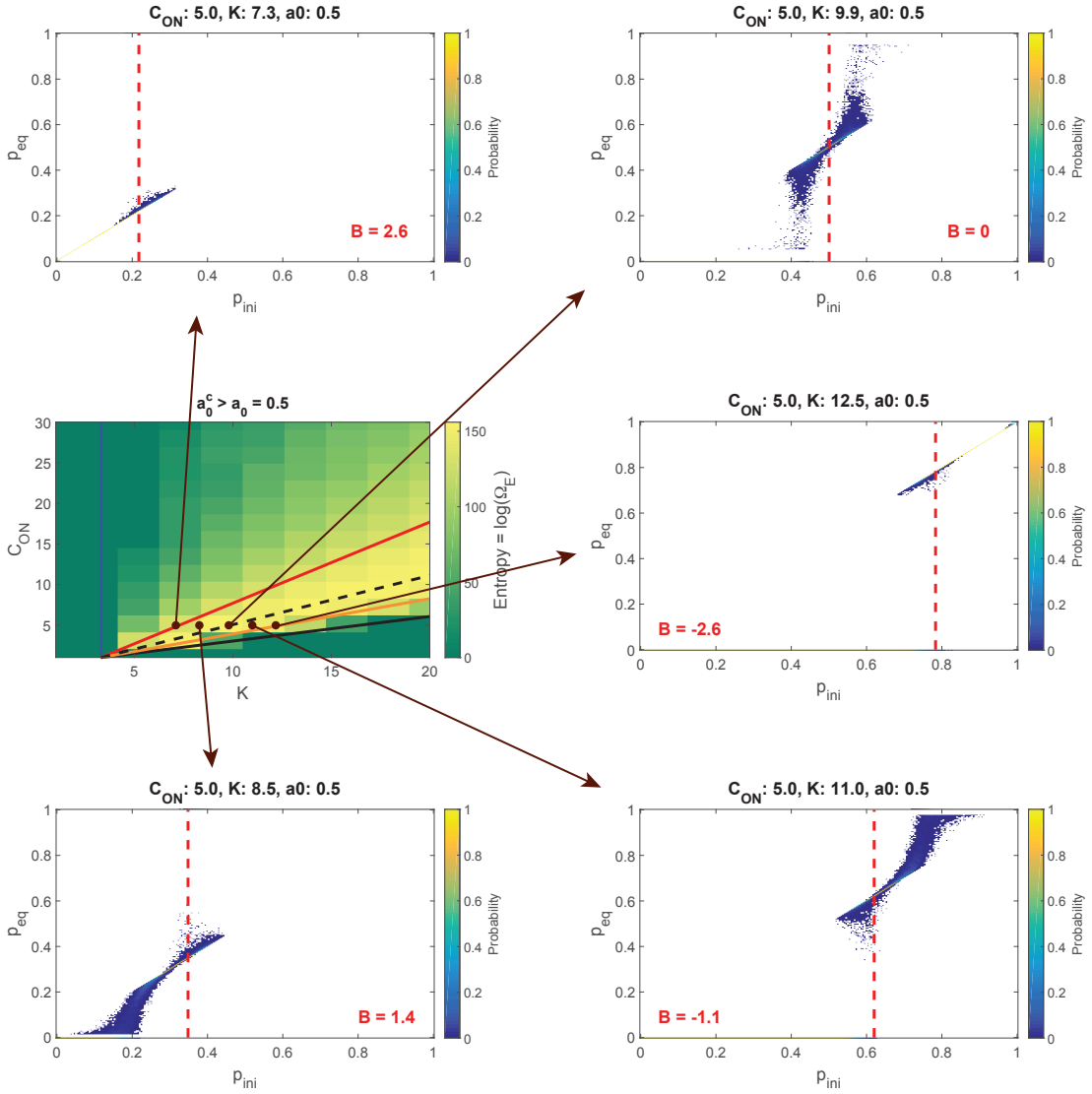

Figure S3: (Related to Figure 3) **Analysis of the activate-deactivate phase using the signal field B.** The heatmap (C_{ON} vs. K) quantifies the multicellular entropy - the total number of equilibrium states as a function of K and C_{ON}, and thus in each behavioural phase (from Maire and Youk, *Cell Systems* (2015)). p_{eq} is the value of p when the cellular automaton terminates (equilibrates) and p_{ini} is the cellular automaton's starting value of p. The red vertical dashed line approximately splits the p_{eq} vs. p_{ini} map into two regions (described by equation S62): (Left side) deactivation is dominant, and (Right side) activation is dominant. In both regions, $\Delta h \leq 0$. These maps indeed show that: (1) When p_{ini} is less than $1/2 - B/(4f_N)$, deactivation occurs ($\Delta p < 0$); (2) When p_{ini} is larger than $1/2 - B/(4f_N)$, activation occurs ($\Delta p > 0$). Therefore, we conclude that the pseudo-energy monotonically decreases in the activate-deactivate phase. All plots here are for $N = 225$ cells (in a 15×15 triangular lattice) with $a_0 = 0.5$ and $R = 0.1$.

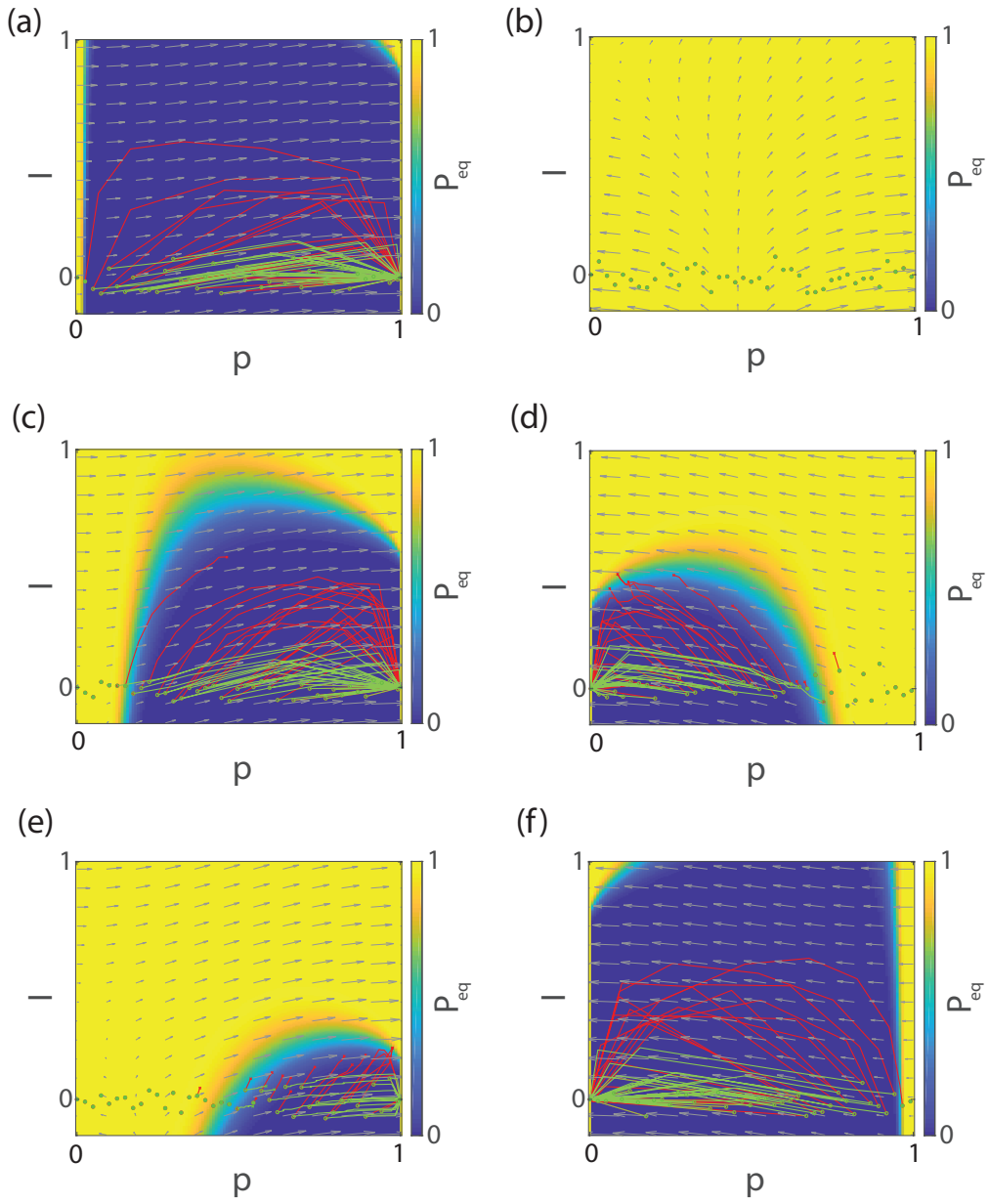

Figure S4: (Related to Figure 4) **Gradient fields of the pseudo-energy, P_{eq}, and particle trajectories - Weak interactions.** Simulated trajectories of the cellular automaton (red lines), together with trajectories of the equation of motion Eq. S82 (green lines), plotted on top of the vector field generated by the negative of the gradient of the pseudo-energy (grey arrows), plotted on top of the 'stickiness' P_{eq} (color bar). Circles represent initial values and crosses values at equilibrium. For the Langevin trajectories, we took the same initial values as generated from the automaton simulations. Weak interaction regime ($a_0 = 1.5$), $N = 121$ cells. (a) Activation, $K = 3, C_{ON} = 24$, (b) Autonomy, $K = 15, C_{ON} = 20$, (c) Activation, $K = 6, C_{ON} = 21$, (d) Deactivation, $K = 17, C_{ON} = 14$, (e) Activation, $K = 10, C_{ON} = 21$, (f) Deactivation, $K = 20, C_{ON} = 14$.

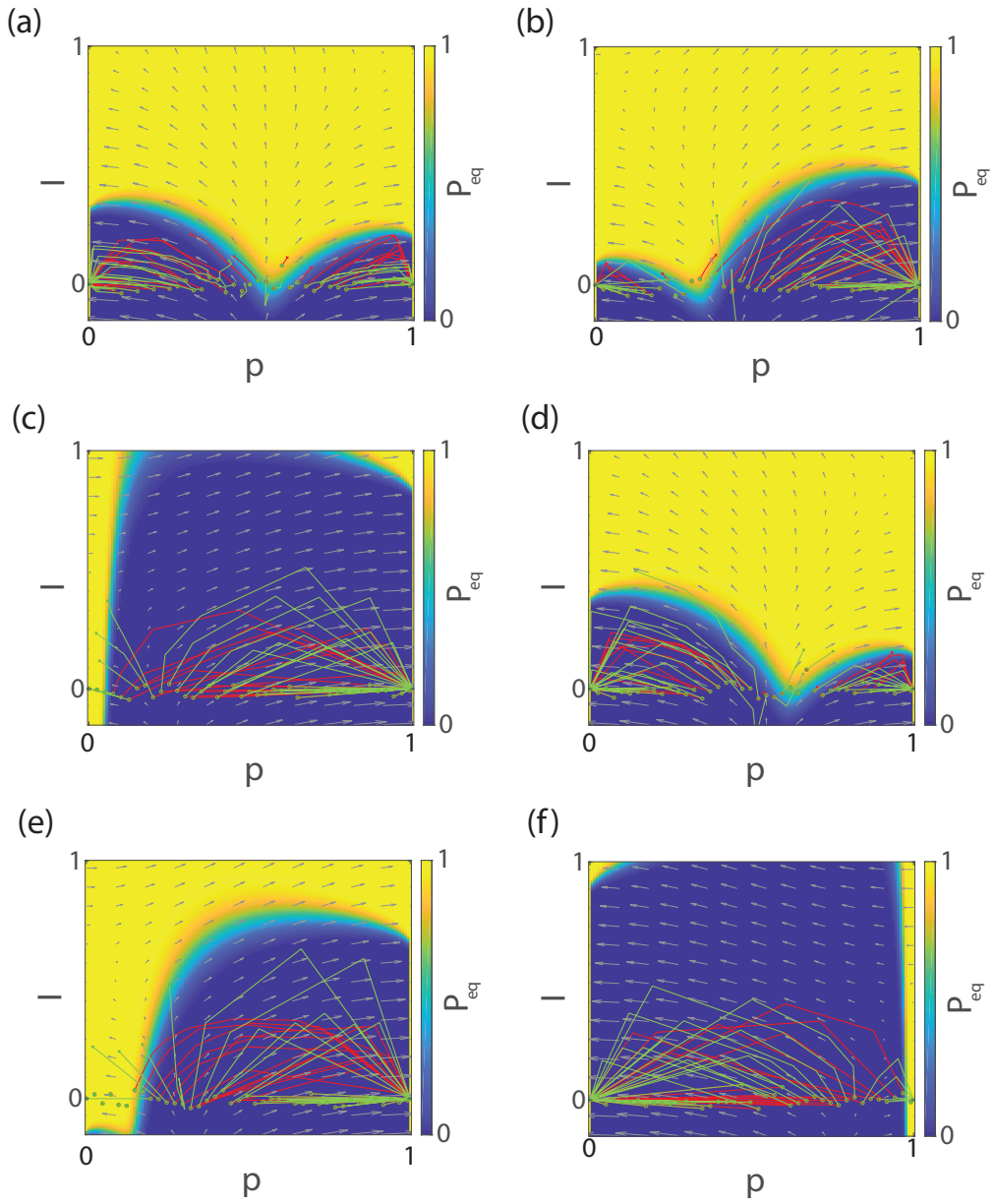

Figure S5: (Related to Figure 4) **Gradient fields of the pseudo-energy, P_{eq}, and particle trajectories - Strong interactions.** Simulated trajectories of the cellular automaton (red lines), together with trajectories of the equation of motion Eq. S82 (green lines), plotted on top of the vector field generated by the negative of the gradient of the pseudo-energy (grey arrows), plotted on top of the 'stickiness' P_{eq} (color bar). Circles represent initial values and crosses values at equilibrium. For the Langevin trajectories, we took the same initial values as generated from the automaton simulations. Strong interaction regime ($a_0 = 0.5$), $N = 121$ cells. (a) Activation-deactivation, $K = 10, C_{ON} = 5$, (b) Activation-deactivation, $K = 19, C_{ON} = 14$, (c) Activation, $K = 10, C_{ON} = 21$, (d) Activation-deactivation, $K = 16, C_{ON} = 8$, (e) Activation, $K = 14, C_{ON} = 16$, (f) Deactivation, $K = 18, C_{ON} = 6$.

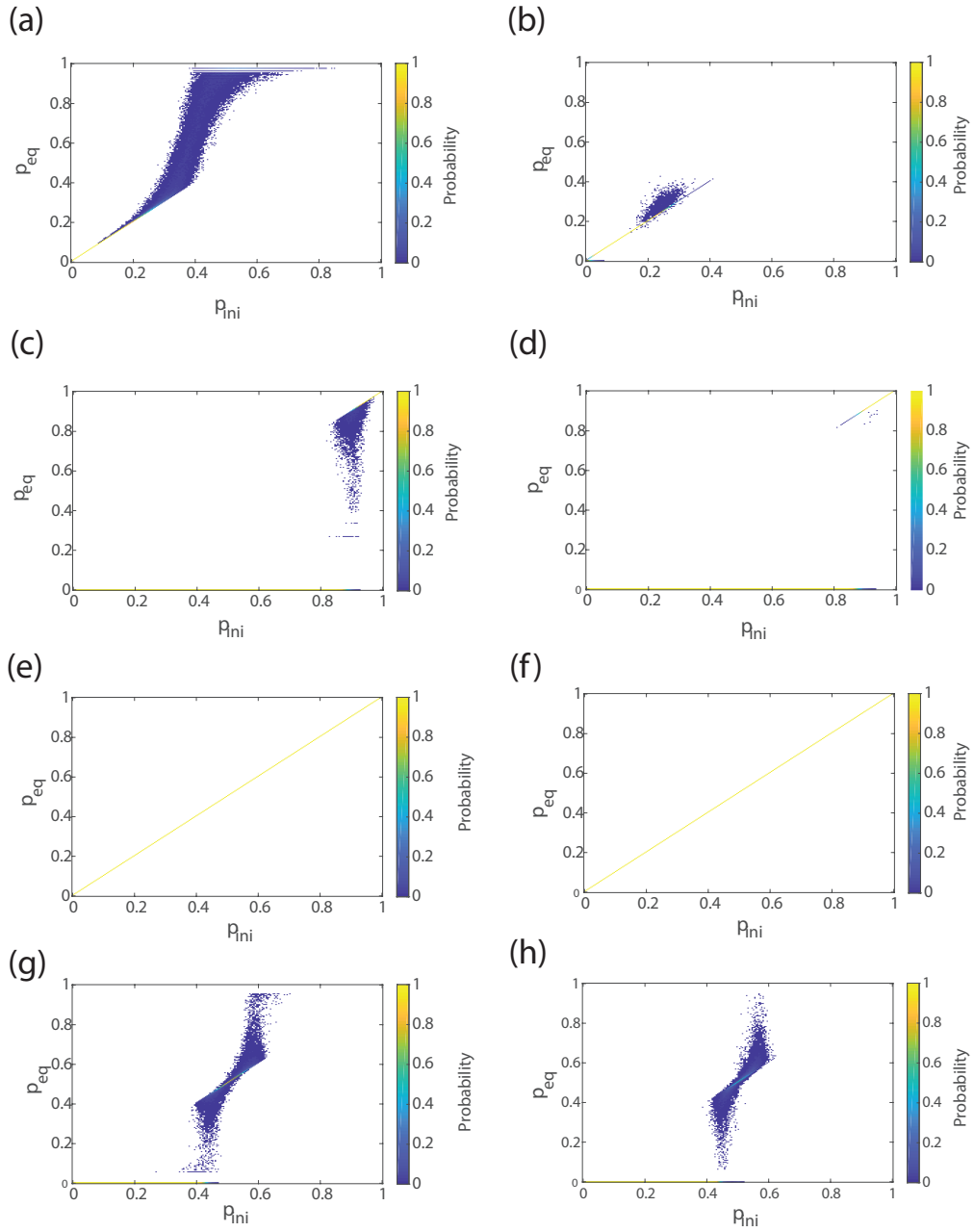

Figure S6: (Related to Figure 4) $p_{initial} - p_{equilibrium}$ **maps for the cellular automaton (left column) and the equation of motion (right column).** For each value of $p = n/N$, we did 1000 trials and determined the value of p for the equilibrium configuration. (a), (b) Activation, $a_0 = 1.5, K = 6, C_{ON} = 15$. (c), (d) Deactivation, $a_0 = 1.5, K = 20, C_{ON} = 15$, (e), (f) Autonomy, $a_0 = 1.5, K = 12, C_{ON} = 15$, (g), (h) Activation-deactivation, $a_0 = 0.5, K = 15, C_{ON} = 8$. For all simulations, $N = 225$ and for each value of p_{ini} we did 1000 simulations.

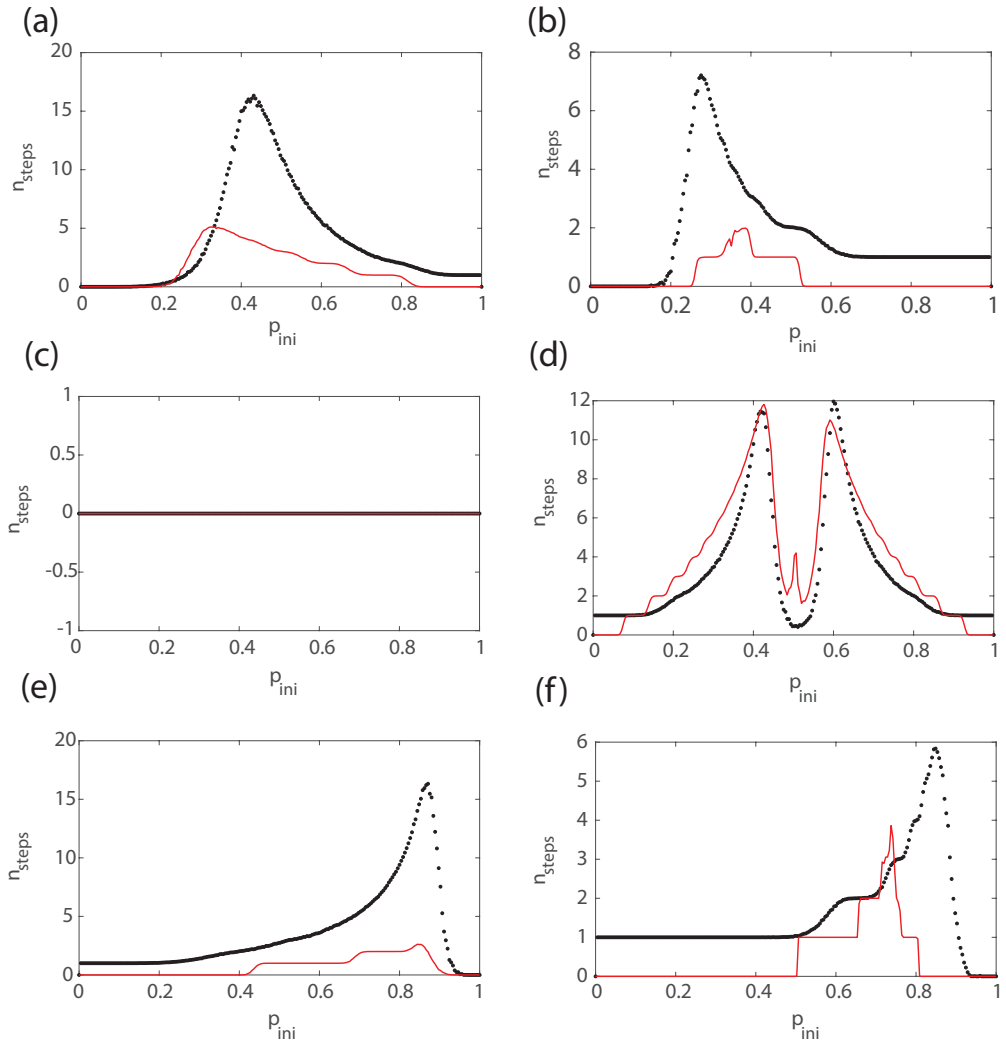

Figure S7: (Related to Figure 4) **Mean equilibration times from the trajectories of the pin-pout maps S6 for the cellular automaton (black dots) and the equation of motion (red line).** Left column: weak interaction ($a_0 = 1.5$), (a) Activation, $K = 6, C_{ON} = 15$, (c) Autonomy, $K = 12, C_{ON} = 15$, (e) Deactivation, $K = 20, C_{ON} = 15$. Right column: strong interaction ($a_0 = 0.5$). (b) Activation $K = 14, C_{ON} = 12$, (d) Activation-deactivation, $K = 15, C_{ON} = 8$, (f) Deactivation, $K = 14, C_{ON} = 5$. For all simulations, $N = 225$.

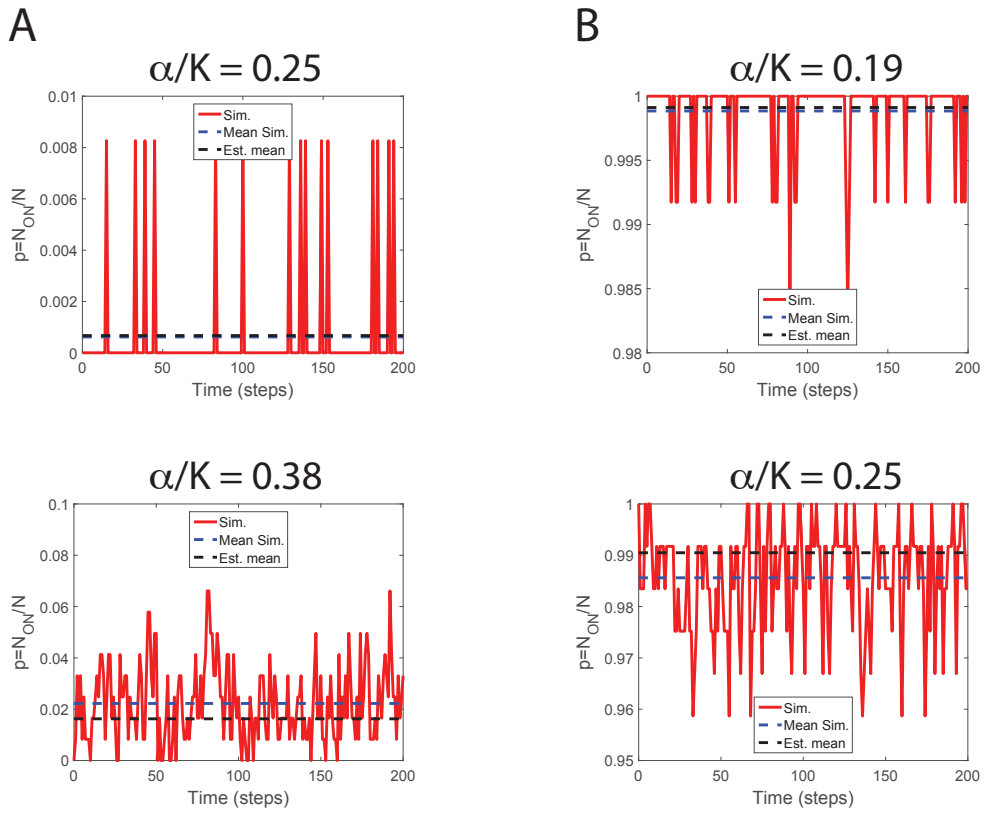

Figure S8: (Related to Figure 5) **Noise perturbs all-ON and all-OFF states. column A. Initial state has all cells OFF.column B. Initial state has all cells ON. Both initial states are steady states of the corresponding deterministic cellular automaton. For all simulations $N = 121$ cells in a 11×11 grid, $R = 0.2a_0$, $a_0 = 0.5$, $K = 16$ and $C_{ON} = 8$ (activate-deactivate phase). Red curves show the dynamics produced by the noisy cellular automaton. Noise strength is α/K. The dashed blue line is the time average of p computed directly from the noisy cellular automaton and the dashed black line is the analytical estimate (equations S108 for column A and S109 for column B.)**

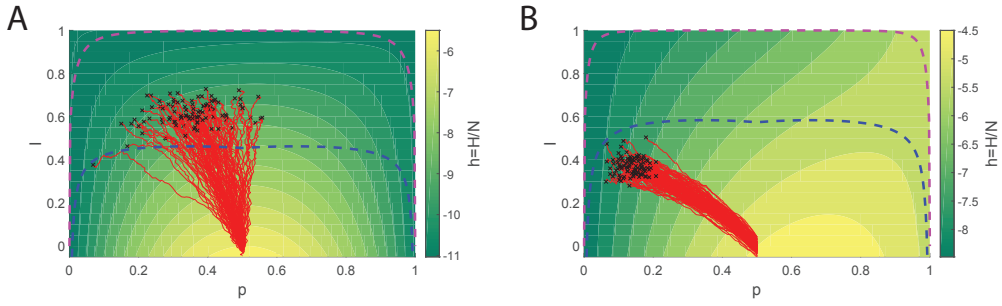

Figure S9: (Related to Figure 5) **Noise-induced particle trajectories on symmetric and asymmetric pseudo-energy landscapes for secrete-and-sense cells that operate in the autonomy phase.** $N = 441$ in a 21×21 grid, $R = 0.2a_0$, $a_0^c \approx 0.97$. The dashed blue line is the estimate of the maximum spatial index from equation S32. The dashed magenta line is the upper bound of the spatial index given by Eq. S48. **A.** 100 particle trajectories, all starting from ($p = 0.5$, $I \approx 0$); $a_0 = 1$, $K = 13$, $C_{ON} = 12$ and a relative noise strength $\alpha/K = 0.15$. **B.** 100 particle trajectories, all starting from ($p = 0.5$, $I \approx 0$); $a_0 = 1.5$, $K = 10$, $C_{ON} = 10$ and a relative noise strength $\alpha/K = 0.1$.

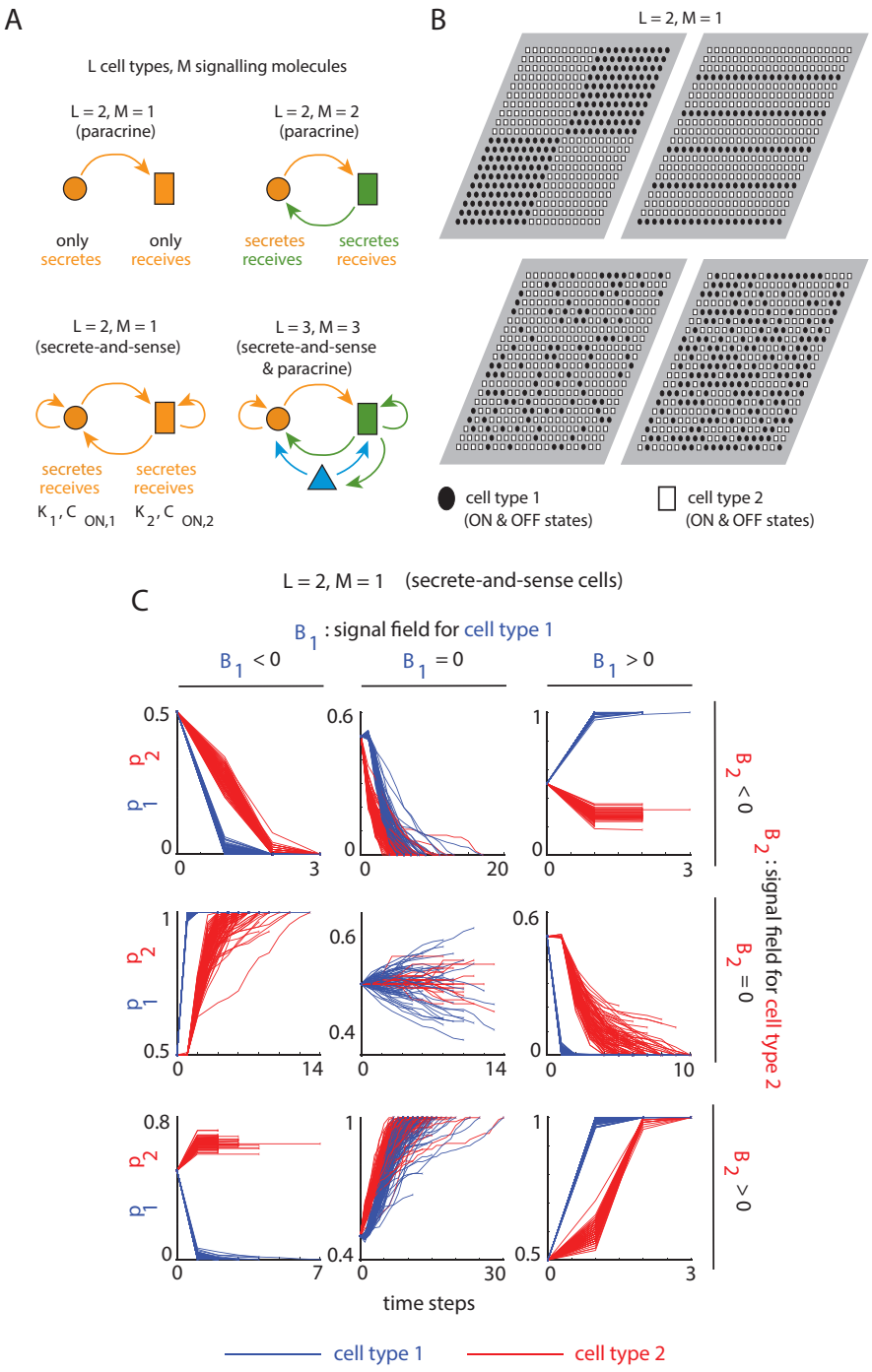

Figure S10: (Related to Figure 5) **Extension to lattices with any number of cell types and signalling molecules (Section S8). A. Examples of secrete-and-sensing and paracrine signalling.** L **types of cells with** M **types of signalling molecules. B. Examples of triangular lattices with two types (**L**=2) of secrete-and-sense cells (circles and rectangles) that share the same signalling molecule (M=1). For each lattice,** $N =$ **400 cells,** a_0**=0.5,** $R = 0.2$**, and** $f_N \approx 2.358$**. Using the formalism detailed in Section S3, we obtain interaction strengths** f_{lm} **between cell-type** l **and cell-type** m**: (top left) -** $f_{11} =$ **0.854,** $f_{12} =$ **0.325,** $f_{22} =$ **0.854; (top right) -** $f_{11} =$ **0.142,** $f_{12} =$ **0.447,** $f_{22} =$ **1.321; (bottom left) -** $f_{11} =$ **0.147,** $f_{12} =$ **0.443,** $f_{22} =$ **1.326; (bottom right) -** $f_{11} =$ **0.585,** $f_{12} =$ **0.594,** $f_{22} =$ **0.585. C. Fraction** p_1 **of cells of type 1 that are ON (blue curves) and fraction** p_2 **of cells of type 2 that are ON (red curves) for cellular automata simulations with two types of secrete-and-sense cells with shared signal (L=2, M=1, N=400,** N_1**=120,** N_2**=280,** a_0**=0.5,** R_1**=**R_2**=0.2**a_0**,** $C_{ON,1}$**=8, and** $C_{ON,2}$**=5). All start with** p_1**=**p_2**=0.5.** B_u **is the signal field for cell type u (u=1, 2). The signs of** B_u **determine cell type** k**'s change in** p_u **over time. If neither** B_1 **nor** B_2 **is zero, then** p_u **increases over time if** $B_u > 0$ **and decreases over time if** $B_u < 0$**. When** $B_u \approx 0$**, then** p_u **nearly stays the same for the first several time steps and then follows the direction of change of the other cell type's** p**.**

Transparent Methods

Contents

S1 Detailed description of the cellular automaton and the interaction strength $f_N(a_0)$

The cellular automaton calculates the concentration c of the signal due to a single cell through the following reaction-diffusion equation:

$$\frac{\partial c}{\partial t} = \nabla \cdot (D \nabla c) - \gamma c + \frac{\eta(c)}{4\pi R^2} \delta (r - R), \tag{S1}$$

where $\eta(c)$ is the secretion rate that depends on the cell's state (i.e., ON or OFF), D is the diffusion constant, γ is the degradation rate of the signal, and R is the radius of the spherical cells. The cellular lattice is two-dimensional but the diffusion is in three dimensions. This is typical of tissues that are embedded in three-dimensional space. We limit ourselves to cells whose time-scale for responding to changes in the concentration of the signal is slower than the time-scale for diffusion to create steady-state signal concentrations. Thus we are only interested in steady state concentration of the signal. The solution for the steady-state, with the boundary condition that $\lim_{r\to\infty} c(r) = 0$ is

$$c(r) = \frac{c_R R}{r} e^{(R-r)/\lambda} \quad \text{,where} \quad c_R = \frac{\eta\gamma}{4\pi R\lambda(\lambda + R)}, \tag{S2}$$

where we define the **diffusion length** $\lambda = \sqrt{D/\gamma}$. By measuring all **distances in units of** λ and **concentrations in units of** c_R **of an OFF cell**, equation S2 simplifies to

$$c(r) = \begin{cases} \frac{R}{r} e^{R-r} & \text{for an OFF cell} \\ C_{ON} \frac{R}{r} e^{R-r} & \text{for an ON cell} \end{cases} \tag{S3}$$

Equation S3 is for one cell. In our normalized units, the steady-state concentration on an OFF cell is 1 and on an ON cell is C_{ON}. For our lattice of N cells, we let each cell be denoted by an index i and let X_i denote cell-i's state (ON or OFF):

$$X_i = \begin{cases} 0 & \text{if the cell-i is OFF} \\ 1 & \text{if the cell-i is ON} \end{cases} \tag{S4}$$

The concentration Y_i of signal on cell-i is

$$Y_i = (C_{ON} - 1) X_i + 1 + \sum_{j \neq i} [(C_{ON} - 1) X_j + 1] f(r_{ij}), \tag{S5}$$

where the summation runs through all the other cells in the lattice, r_{ij} is the distance between the centers of cell-i and cell-j, and $f(r_{ij})$ is

$$f(r_{ij}) = \frac{1}{4\pi R^2}\int_{\text{cell-i}} \frac{Re^{R-r}}{r} dA = \frac{e^{R-r_{ij}}}{r_{ij}} \sinh(R) \tag{S6}$$

The term $(C_{ON}-1)\,X_i + 1$ in equation S5 comes from equation S3. In writing equation S5, we are assuming that the cells average the concentration of the signal on their surfaces. Note that if $R << \lambda$, then $\sinh(R) \approx R$. In this case, we can calculate the concentration due to cell-j on cell-i by simply calculating $c(r_{ij})$ as given in the equation S3. Based on equation S3, we can write the concentration $c_i(r)$ created solely cell-i in terms of Y_i, C_{ON} and K as:

$$c_i(r) = \begin{cases} \frac{R}{r}e^{R-r} & \text{if } Y_i < K \\ C_{ON}\frac{R}{r}e^{R-r} & \text{if } Y_i \geq K \end{cases} \tag{S7}$$

Motivated by $f(r_{ij})$ in equation S5, let us define an important quantity f_N, which we call the **interaction strength**,

$$f_N\,(a_0) \equiv \sum_{j\neq i} \frac{e^{R-r_{ij}}}{r_{ij}} \sinh(R) \tag{S8}$$

The interaction strength f_N is the same for every cell on the lattice because we are using a periodic boundary condition, in which top edge is joined with the bottom edge and the left edge is joined with a right edge (i.e. we are modelling a closed tissue). Our previous work (Maire and Youk, *Cell Systems* (2015)) showed how the f_N , K, and C_{ON} together determine the behavioural phase of the cellular lattice (Fig. 1(b) in the main text).

In the cellular automaton, We treat the state of the cellular lattice as a vector $\vec{X} = [X_1, \ldots, X_N]$ where, for each cell i, X_i is given by equation S4. This determines the configuration of the population (i.e. its spatial pattern), with each cell being either ON or OFF. There are 2^N possible configurations. Given a state $\vec{X}$, we calculate the concentration sensed by each cell i (denoted Y_i) through equation S5. We can write this in a vector notation as $\vec{Y} = [Y_1, \ldots, Y_N]$, where

$$\vec{Y} = M\left[(C_{ON}-1)\vec{X} + \vec{1}\right] \tag{S9}$$

with $\vec{1}$ being the identity vector of ones and the elements of the matrix M are given by

$$M_{ij} = \begin{cases} 1 & \text{if } i = j \\ \frac{e^{R-r}}{r}\sinh(R) & \text{if } i \neq j \end{cases} \tag{S10}$$

For each time step t in the cellular automaton, we have an initial configuration $\vec{X}_t$ and we calculate the vector $\vec{Y}$ at time t, denoted $\vec{Y}_t$. Then we calculate the new configuration $\vec{X}_{t+1}$ according to equation S4. This defines the dynamics of our system.

S2 Properties of the spatial index I

S2.1. Derivation of the spatial index I in terms of p

The **spatial index**, I is a modified version of the Moran index (i.e., Moran's I). It is a weighted, spatial autocorrelation of the cell states whereby each cell pair (i, j) is weighted by the interaction strength $f_N(r_{ij})$ for that pair. Specifically, we defined I in the main text as

$$I = \frac{N}{\sum_i \sum_{j\neq i} f\,(r_{ij})} \frac{\sum_i \sum_{j\neq i} f\,(r_{ij})\,(X_i - \langle X\rangle)\,(X_j - \langle X\rangle)}{\sum_i (X_i - \langle X\rangle)^2} \tag{S11}$$

where $f\,(r_{ij})$ is the term in the interaction strength for the cell-pair $(i,\, j)$: $f\,(r_{ij}) = \frac{e^{R-r_{ij}}}{r_{ij}} sinh(R)$ (this is denoted by $g(r_{ij})$ in the main text). Moreover, X_i is defined by

$$X_i = \begin{cases} -1 & \text{if cell-i is OFF} \\ 1 & \text{if cell-i is ON} \end{cases} \tag{S12}$$

which is different from the previous definition of X_i (equation S4). In the remainder of this supplementary text, we will use this definition of X_i for reasons that will become clearer in the following sections. Note that this definition does not change the features of our model because our previous definition of X_i is related to this revised definition of X_i by a linear relation[1].

In terms of p, we have X_i is $\langle X \rangle = 2p - 1$ and $\sum_i (X_i - \langle X \rangle)^2 = 4Np(1-p)$. Moreover, by the definition of the interaction strength (equation S8), we have $\sum_{j \neq i} f(r_{ij}) = f_N$. Therefore

$$I = \frac{1}{f_N} \frac{\sum_i \sum_{j \neq i} f(r_{ij}) X_i X_j - 2(2p-1) \sum_i \sum_{j \neq i} f(r_{ij}) X_i + (2p-1)^2 N f_N}{4Np(1-p)}$$

where we used the fact that $f(r_{ij}) = f(r_{ji})$. Note that

$$\sum_i \sum_{j \neq i} f(r_{ij}) X_i = N \langle \sum_{j \neq i} f(r_{ij}) X_i \rangle = N f_N \langle X \rangle = N f_N (2p-1)$$

where the brackets denote averaging among all cells. Combining above results, we have

$$I = \frac{\langle \sum_{j \neq i} f(r_{ij}) X_i X_j \rangle - (2p-1)^2 f_N}{4p(1-p) f_N} \tag{S13}$$

where we have used $\sum_i \sum_{j \neq i} f(r_{ij}) X_i X_j = N \langle \sum_{j \neq i} f(r_{ij}) X_i X_j \rangle$. Note that f_N is a purely geometric quantity that is almost constant when N is sufficiently large due to $f(r_{ij})$ scaling as $e^{-r_{ij}}$. This is precisely equation 2 in the main text. For later use, we also define

$$\Theta = \frac{1}{N} \sum_i \sum_{j \neq i} f(r_{ij}) X_i X_j \tag{S14}$$

With this, we can write

$$I = \frac{\Theta(X) - (2p-1)^2 f_N}{4p(1-p) f_N} \tag{S15}$$

S2.2 Spatial index I in the limits $p \to 0$ and $p \to 1$

Let $X = (X_1, \ldots, X_N)$ be a microstate, with $X_i \in \{-1, 1\}$. Note that I is undefined when $p = 0$ or $p = 1$ because both denominator and nominator vanish in the Eq. S11. So we can only discuss what I becomes in the limit of $p \to 0$ and $p \to 1$. Let us consider the limit $p \to 0$ (same argument applies to $p \to 1$). Given that p is a discrete variable for a fixed value of N, taking the limit $p \to 0$ means that we consider the value of I at $p = 1/N$, which is the lowest possible non-zero value of p. For a lattice with N cells, there are N microstates with $p = 1/N$. In these states, all but one cell is OFF. Let $X_1 = 1, X_{i \neq 1} = -1$, then

$$\begin{aligned} \Theta(X) &= \frac{1}{N} \sum_{j \neq 1} f(r_{1j}) X_1 X_j + \frac{1}{N} \sum_{i=2}^{N} \sum_{\substack{j=2 \\ j \neq i}}^{N} f(r_{ij}) X_i X_j = \frac{1}{N} (-f_N + \sum_{i=2}^{N} \sum_{\substack{j=2 \\ j \neq i}}^{N} f(r_{ij})) \\ &= \frac{1}{N} (-f_N + \sum_{i=2}^{N} (f_N - f(r_{i1}))) = \frac{1}{N} (-f_N + (N-2) - f_N) = \frac{N-4}{N} f_N \end{aligned} \tag{S16}$$

Also, $p = 1/N$ and thus

$$I = \frac{\frac{N-4}{N} f_N - \frac{(N-2)^2}{N^2} f_N}{\frac{4(N-1)}{N^2} f_N} = \frac{(N-4)N - (N-2)^2}{4(N-1)} = -\frac{1}{N-1}$$

For typical lattice sizes that we study (e.g., $N = 225$), above equation tells us that $I \sim -0.001$, which is practically zero. Moreover, we see that for $N \to \infty, I \to 0$. In fact, for $N \to \infty$, we also have $p \to 0$ for this configuration. For these reasons, we set $I = 0$ when $p \to 0$ in our study. The same holds for the limit $p \to 1$. Thus, defining $I = 0$ for a uniform lattice seems to be a reasonable choice and ensures continuity in the limit of $N \to \infty$.

[1] $2X_i^{\text{old}} = X_i^{\text{new}} + 1$

S2.3 Upper bound for the spacing between allowed values of I

To justify the fact that in the macroscopic equation of motion (Section S6) we take (p, I) to be continuous, we show in this section that the spacing between possible values of I is bound by a value that goes to zero in the limit $N \to \infty$. Note that the spacing in allowed values of p is $1/N$ and therefore trivially goes to zero. Determining the spectrum of allowed values of I for a fixed p is a notably harder problem, which we will not tackle in detail here. Rather, we will only derive an upper bound that goes to zero in the large system size limit, for any p not too close to zero or one (more on this later).

Consider a microstate with $p \neq 0$, $p \neq 1$ and consider two cells k and l. Suppose $X_k \neq X_l$, i.e. one of them is an ON-cell and the other an OFF-cell. We will consider what happens to I if we flip both cells, i.e. $X_k \to -X_k$ and $X_l \to -X_l$ (here we take $X_i \in \{-1, 1\}$). Clearly, the fraction of ON-cells does not change, so p remains constant. For the change in Θ, let us first write

$$N\Theta = \sum_{i\neq k,l} \sum_{j\neq i,k,l} f(r_{ij}) X_i X_j + 2\sum_{j\neq k} f(r_{kj}) X_k X_j + 2\sum_{j\neq l} f(r_{lj}) X_l X_j - 2f(r_{kl}) X_k X_l \tag{S17}$$

The factors 2 come from the fact that each interaction is counted twice in the definition of Θ (Eq. S14). Here we have separated the terms of Θ into four terms, of which only the middle two change when we flip the states of cells k and l. Hence we have

$$N\Delta\Theta \equiv N(\Theta_{new} - \Theta_{old}) = -4\sum_{j\neq k} f(r_{kj}) X_k X_j - 4\sum_{j\neq l} f(r_{lj}) X_l X_j \tag{S18}$$

Since $|X_i| = 1$ for all cells and $|\sum_{j\neq k} f(r_{kj})| \leq \sum_{j\neq k} |f(r_{kj})| = f_N$, we obtain

$$\begin{aligned} |N\Delta\Theta| &\leq 4|\sum_{j\neq k} f(r_{kj}) X_k X_j| + 4|\sum_{j\neq l} f(r_{lj}) X_l X_j| \leq 8|\sum_{j\neq k} f(r_{kj}) X_k X_j| \\ &\leq 8\sum_{j\neq k} |f(r_{kj}) X_k X_j| \leq 8\sum_{j\neq k} |f(r_{kj})||X_k||X_j| = 8f_N \end{aligned} \tag{S19}$$

Finally, let $\Delta I = I_{new} - I_{old}$. Since p does not change, we have

$$|\Delta I| = \left| \frac{\Delta\Theta}{4f_N p(1-p)} \right| \leq \frac{2}{Np(1-p)} \tag{S20}$$

This calculation shows that starting from an arbitrary lattice in which not all cells are ON or OFF, it is always possible to generate a different cellular lattice with the same p, of which the value of I differs by no more than $\frac{2}{Np(1-p)}$. In the limit of $N \to \infty$, this value goes to zero whenever p is not too close to 0 or 1. Therefore, as long as we are away from the boundaries, we can safely take I to be continuous in the limit of large system size.

For p close to zero and one, the bound might be very large (but note that the above argument excludes the extremes $p = 0$ and $p = 1$). However, there are very few different values of I that are possible near these bounds. For instance, for a single ON-cell in a lattice of OFF cells there is only one value of I possible. For two ON-cells, the number of unique values equals the number unique distances possible between two cells. As we argued in the main text and in the previous section, the value of I becomes irrelevant in these limits as there are only one or a few values possible. Nevertheless, we should be careful when considering the value of I near these bounds.

S3 Deriving the maximum allowed value of $|I|$ for each p: $|I_{max}(p)|$

S3.1. Deriving $I_{max}(p)$ (dashed black curves in Figs. 3 and 5) via a mean-field approach

We now use a mean-field approach, in which we treat each cell's nearest neighbours exactly and treat the more distant neighbours through a mean-field approximation. Specifically, we can write the signal concentration sensed by cell-i due to all the other cells, denoted Y_i^{nei}, as

$$Y_i^{\text{nei}} = f(a_0)\left[(C_{ON}-1)\,m_i + 6\right] + \sum_{\substack{j\neq i \\ r_{ij}>a_0}} f(r_{ij})\left[(C_{ON}-1)\,\frac{(X_j+1)}{2}+1\right] \tag{S21}$$

where $f(r_{ij})$ is the term in the interaction strength for the cell-pair (i,j), and $f(a_0) = \frac{\sinh R}{a_0} e^{R-a_0}$. m_i is the number of nearest neighbours of cell-i that are ON. Let p be the fraction of cells that are ON in the lattice. We can then approximate the last term of equation S21 as

$$\sum_{\substack{j\neq i \\ r_{ij}>a_0}} f(r_{ij})\left[(C_{ON}-1)\,\frac{(X_j+1)}{2}+1\right] \approx \left(f_N - 6f(a_0)\right)\left[pC_{ON} + (1-p)\right]$$

We use a polygon to enclose each island of ON-cells. The polygons are constructed by putting a line between an ON and an OFF cells that are adjacent to each other. Our analysis here is similar to the one that is used for understanding the 2D Ising model near its critical temperature. Given that all polygons are closed, the average number $\langle m_{i=ON}\rangle$ of ON nearest neighbours that surround each ON-cell is

$$\langle m_{i=ON}\rangle = 6 - \frac{\sum_{\{\nu\}} L_\nu}{\sum_{\{\nu\}} A_\nu} \tag{S22}$$

where the sum $\sum_{\{\nu\}}$ runs over all the polygons in the cellular lattice. Here we used the fact that $\sum_{\{\nu\}} A_\nu = pN$, which is the total number of ON cells in the lattice. We have seen that $\langle m_{i=ON}\rangle$ monotonically increases over time. According to equation S22, $\langle m_{i=ON}\rangle$ can only monotonically increase over time if and only if $\frac{\sum_{\{\nu\}} L_\nu}{\sum_{\{\nu\}} A_\nu}$ decreases over time. This is only possible if the polygonal islands of ON cells progressively grow over time to become larger polygonal islands of ON cells. This implies that OFF cells also group together into domains. This is how spatial index increases over time.

We now use $\langle m_{i=ON}\rangle$ to obtain an analytical estimate of $I(t)$. First note that

$$N\langle \sum_{j\neq i} f\left(r_{ij}\right) X_i X_j\rangle = \sum_i \sum_{j\neq i} f\left(r_{ij}\right) X_i X_j = \sum_{i=ON}\sum_{j\neq i} f\left(r_{ij}\right) X_j - \sum_{i=OFF}\sum_{j\neq i} f\left(r_{ij}\right) X_j \tag{S23}$$

in terms of the average number of nearest ON neighbors. Taking m_i to be the number of nearest neighbours that are ON, we have

$$\sum_{j\neq i} f\left(r_{ij}\right) X_j = f(a_0)(2m_i - 6) + \sum_{\substack{j\neq i \\ r_{ij}>a_0}} f(r_{ij}) X_j \approx f(a_0)(2m_i-6) + \left(f_N - 6f(a_0)\right)(2p-1) \tag{S24}$$

where we used the mean-field approach for a cell's interaction with its non-nearest neighbours. Using equations S24 and S23, we obtain

$$N\langle \sum_{j\neq i} f\left(r_{ij}\right) X_i X_j\rangle \approx 2f(a_0)\left(\sum_{i=ON} m_i - \sum_{i=OFF} m_i\right) - 6N(2p-1)f(a_0) + N(f_N - 6f(a_0))(2p-1)^2 \tag{S25}$$

where we have used the fact that $\sum_{i=ON} 1 - \sum_{i=OFF} 1 = N(2p-1)$. We can simplify this equation by noting that $\sum_{i=ON} m_i = pN\langle m_{i=ON}\rangle$, $\sum_{i=OFF} m_i = (1-p)N\langle m_{i=OFF}\rangle$ and that

$$\langle m_i\rangle = 6p = p\langle m_{i=ON}\rangle + (1-p)\langle m_{i=OFF}\rangle \tag{S26}$$

This leads to

$$\langle \sum_{j\neq i} f\left(r_{ij}\right) X_i X_j\rangle \approx 4pf(a_0)\langle m_{i=ON}\rangle - 4pf_N\left(1 - p + 6p\frac{f(a_0)}{f_N}\right) + f_N \tag{S27}$$

By equation S27 and Equation 2 in the main text, we obtain

$$I(t) \approx \frac{\left(\langle m_{i=ON}(t)\rangle - 6p(t)\right) f(a_0)}{(1-p(t))f_N} \tag{S28}$$

This is our analytical formula for the spatial index I as a function of time. Equation S28 underestimates I because it uses the mean-field approximation for the interactions with the non-nearest neighbours. The mean-field approximation is not valid when the configuration has a high spatial index. The nearest neighbour approximation is however a good proxy for understanding why the spatial configurations become more organised over time. In particular, if ON- and OFF-cells are randomly distributed over the lattice, then $\langle m_{i=ON} \rangle = \langle m_i \rangle = 6p$ and I would be close to zero.

Now we can estimate the maximum possible value of I as a function of p. Let us first rewrite I using equations S26 and S28 as

$$I \approx \frac{(6p - \langle m_{i=OFF} \rangle)\, f(a_0)}{p f_N} \tag{S29}$$

Now suppose that most cells are OFF and that we want to find an upper bound for $\langle m_{i=ON} \rangle$. We can use the aforementioned polygons and equation S22 to do so. To maximize I, we need to maximize $\langle m_{i=ON} \rangle$ for a fixed p. This means that we need to minimize the total perimeter of the polygons that enclose the ON-cells. We can do this if all the ON-cells reside inside a single polygonal cluster. This single polygon would approximately be a $\sqrt{n} \times \sqrt{n}$ grid of ON cells, with n being the number of ON-cells. In this case, every corner of the polygon is formed by either 3 or 4 sides. Thus such a polygon would have in total 14 sides. The other cells in the boundary of the polygon each contribute 2 sides. Hence, we have a perimeter

$$L = 6 + 8\sqrt{n} = 6 + 8\sqrt{pN}$$

which leads to the following estimate for the maximum value for I using equations S22 and S28:

$$I^{ON}_{\max} \approx \left(6(1-p) - \frac{6}{pN} - \frac{8}{\sqrt{pN}}\right) \frac{f(a_0)}{(1-p) f_N} \tag{S30}$$

We can use a similar approach for a cluster of OFF-cells surrounded by ON cells. Using equation S29, we obtain

$$I^{OFF}_{\max} \approx \left(6p - \frac{6}{(1-p)N} - \frac{8}{\sqrt{(1-p)N}}\right) \frac{f(a_0)}{p f_N} \tag{S31}$$

Combining equations S30 and S31, we obtain an estimate of the **maximum value that a spatial index I can have for a fixed p**:

$$I_{\max} = \max\left(I^{ON}_{\max}, I^{OFF}_{\max}\right) \tag{S32}$$

Plotting this in the the phase space yields the dashed black curves shown in Fig. 3. Note that the actual maximum value of I is typically higher than our estimate here because we have ignored spatial organization of cells up to second- or third-nearest neighbours. Thus the actual trajectories of the particles in the phase space would go slightly beyond the $I_{\max}$ (Figs. 3b-3e - dashed black curves).

S3.2. More accurate estimate of $I_{max}(p)$ (the dashed orange curve in Fig. 5c)

When the population is highly organised, the above estimated maximum value of I does not agree well with the exact values of I from the cellular automaton runs. In this section, we deduce a more accurate upper bound for the spatial index I, shown in Fig. 3f as an orange dashed line, by exactly treating interactions with more distance neighbors than the nearest neighbors.

First, we must approximate the signaling strength for any arbitrary distributions of cells, including arrangements of cells that do not have any regularity (i.e., non-lattices). Take any cell-i among a group of N cells that may be arranged in any arbitrary manner. We want to know how the neighbours of this cell are continuously distributed in space. Let us take a thin (width $\mathrm{d}r \to 0$) circle with radius r centered at cell-i (see Fig. S2) and count how many cells we find inside this circle. To simplify the analysis, we assume that all cells are point-like cells. Suppose we count n cells in the circle. The number density $g(r)$ is then defined by n divided by the area of the circle:

$$g_i(r) = \frac{n}{2\pi r \mathrm{d}r} \tag{S33}$$

Therefore we have

$$N - 1 = 2\pi \int_0^\infty g_i(r) r \mathrm{d}r \tag{S34}$$

where cell-i is not counted in $g_i(r)$. Applying periodic boundary conditions, all cells have the same $g_i(r) = g(r)$ which we pick to be delta functions to capture the exact positions of the cells:

$$g(r) = \frac{1}{2\pi r} \sum_{j \neq i} \delta(r - r_{ij}) \tag{S35}$$

To calculate the interaction strength, we use the function $f(r)$ defined in equation S6, which is the signal concentration on cell-i due to cell-j:

$$f(r) = \frac{e^{R-r}}{r} \sinh(R) \tag{S36}$$

The interaction strength is then

$$f_N = 2\pi \int_0^\infty f(r) g(r) r \mathrm{d}r = G \int_0^\infty g(r) e^{-r} \mathrm{d}r \tag{S37}$$

with G being a constant given by

$$G = 2\pi e^R \sinh(R) \tag{S38}$$

This scheme provides a way to extend the concept of interaction strength to arbitrary distributions of cells. Using equation S37, we can approximate the interaction strength without calculating the entire sum in equation S8. We assume each cell to be located inside inside a hexagon of area

$$A_{\text{cell}} = \frac{\sqrt{3}}{2} a_0^2 \tag{S39}$$

For each cell-i, we assume that the remaining cells form a continuous tissue represented by a number density $g(r)$ that is inversely proportional to the area A_{cell} that one cell occupies. $g(r)$ is zero inside the area occupied by cell-i and for $r > L$, where L is determined by the number of cells. Specifically,

$$g(r) = \begin{cases} A_{\text{cell}}^{-1} & \text{if } 0.5a_0 < r < L \\ 0 & \text{otherwise} \end{cases} \tag{S40}$$

with L satisfying equation S35. In other words,

$$N - 1 = \frac{2\pi}{A_{\text{cell}}} \int_{0.5a_0}^{L} r \mathrm{d}r \implies L = \sqrt{\frac{(N-1)A_{\text{cell}}}{\pi} + (0.5a_0)^2} \tag{S41}$$

We can then estimate the interaction strength as

$$f_N^{\text{est}} = \frac{G}{A_{\text{cell}}} \int_{0.5a_0}^{L} e^{-r} \mathrm{d}r = \frac{G}{A_{\text{cell}}} \left(e^{-0.5a_0} - e^{-L} \right) \tag{S42}$$

To improve our estimate, let us treat the nearest neighbours exactly. They are located at a distance a_0. We treat all the other cells (non-nearest neighbours) as a continuum as before. We then have

$$f_N = 6f(a_0) + \frac{G}{A_{\text{cell}}} \left(e^{-1.5a_0} - e^{-L} \right) \tag{S43a}$$

$$L = \sqrt{\frac{(N-7)A_{\text{cell}}}{\pi} + (1.5a_0)^2} \tag{S43b}$$

Now, suppose we pick a particular ON-cell (OFF-cell). Now, let us count the total number of ON-cells (OFF-cells) that lie within a distance L_{ON} (L_{OFF}) from this particular cell, with the L_{ON} (L_{OFF}) given by the total number of ON-cell (OFF-cells) in the lattice. We proceed by counting the OFF-cells (ON-cells). Then we have

$$\sum_i \sum_{i \neq j} f(r_{ij}) X_i X_j = \sum_{i=ON} \sum_{i \neq j} f(r_{ij}) X_j - \sum_{i=OFF} \sum_{i \neq j} f(r_{ij}) X_j \tag{S44}$$

We can rewrite above using the same approach as in equation S43, but this time we distinguish the contributions of ON- and OFF-cells:

$$\sum_{i=ON} \sum_{i \neq j} f(r_{ij}) X_i X_j \approx 6pNf(a_0) + pN \frac{G}{A_{\text{cell}}} \left(e^{-1.5a_0} - 2e^{-L_{ON}} + e^{-L} \right) \tag{S45a}$$

$$L_{ON} = \sqrt{\frac{(pN-7)A_{\text{cell}}}{\pi} + (1.5a_0)^2} \tag{S45b}$$

with L given in equation S43. For OFF-cells, we have

$$\sum_{i=OFF} \sum_{i \neq j} f(r_{ij}) X_i X_j \approx -6(1-p)Nf(a_0) - (1-p)N \frac{G}{A_{\text{cell}}} \left(e^{-1.5a_0} - 2e^{-L_{OFF}} + e^{-L} \right) \tag{S46a}$$

$$L_{OFF} = \sqrt{\frac{((1-p)N-7)A_{\text{cell}}}{\pi} + (1.5a_0)^2} \tag{S46b}$$

Doing the same for OFF-cells and substituting into equation S44, we find that

$$\langle \sum_{i \neq j} f(r_{ij}) X_i X_j \rangle = f_N - 2G \left(pe^{-L_{ON}} + (1-p)e^{-L_{OFF}} - e^{-L} \right) \tag{S47}$$

Substituting into Equation 2 in the main text yields the upper bound on I as a function of p:

$$I_{\max} = \frac{f_N - 2G \left(pe^{-L_{ON}} + (1-p)e^{-L_{OFF}} - e^{-L} \right) - (2p-1)^2 f_N}{4p(1-p)f_N} \tag{S48}$$

Notice that this upper bound can never be reached by the secrete-and-sense cells because we computed the $I_{\max}$ by assuming the "perfect separation" among ON- and OFF-cells. This cannot be true for every cell simultaneously. Hence, we expect that the value of I for highly organised spatial configuration to lie between the first estimate of $I_{max}(p)$ based on the nearest neighbours approach (Equation S32) and the estimate given by equation S48. This is indeed true as seen in the particle trajectories terminating between the two bounds (Fig. 3f - red trajectories terminate within the region bounded by the black and the orange curves).

S4 Proof that the pseudo-energy h is a non-increasing function over time

Here we show that the pseudo-energy h monotonically decreases over time (i.e., h decreases in the next time step provided that the cellular automaton does not terminate in the current time step). In this section, we will use $H = hN$ for the proof. Note that H evolves over time according to

$$\Delta H = \sum_m \frac{\partial H}{\partial X_m} \Delta X_m \tag{S49}$$

The first term can be written as

$$\frac{\partial H}{\partial X_m} = -\frac{\partial}{\partial X_m} \sum_i X_i (Y_i - K) = -\sum_i \left[\delta_{im} (Y_i - K) + X_i \frac{\partial Y_i}{\partial X_m} \right] \tag{S50}$$

where δ_{ij} is the Kronecker delta. We also have

$$\frac{\partial Y_i}{\partial X_m} = \frac{\partial}{\partial X_m} \left[\left(\frac{C_{ON}-1}{2} \right) \left(X_i + \sum_j f(r_{ij}) X_j \right) + \left(\frac{C_{ON}+1}{2} \right) (1 + f_N) \right] \tag{S51}$$

where $f(r_{ij})$ is the term for the cell pair (i, j) in the interaction strength function. We can rewrite above as

$$\frac{\partial Y_i}{\partial X_m} = \left(\frac{C_{ON} - 1}{2}\right) [\delta_{im} + f(r_{im})] \tag{S52}$$

From this, we obtain

$$\sum_i X_i \frac{\partial Y_i}{\partial X_m} = \left(\frac{C_{ON} - 1}{2}\right) \left(X_m + \sum_i f(r_{im}) X_i\right) = Y_m - \left(\frac{C_{ON} + 1}{2}\right) (1 + f_N) \tag{S53}$$

Finally, using equations S49, S50 and S53, we obtain

$$\Delta H = -2 \sum_m \Delta X_m (Y_m - K) + \sum_m \Delta X_m \left(\frac{C_{ON} + 1}{2}(1 + f_N) - K\right) \tag{S54}$$

Given the definition of X_i, ΔX_i can take on one of three values:

$$\Delta X_i = \begin{cases} -2 & \text{if cell-i is ON and } Y_i < K \\ 2 & \text{if cell-i is OFF and } Y_i > K \\ 0 & \text{otherwise} \end{cases} \tag{S55}$$

Looking at each of the three values case by case, we see that $\Delta X_m (Y_m - K) \geq 0$ for all cells. If $B = 0$ then $\Delta H \leq 0$. Moreover, we expect $\Delta H \leq 0$ for all $B \approx 0$. Therefore, we want to analyze the dynamics of the secrete-and-sense cells for values of C_{ON} and K that yield $B \approx 0$. The values of K and C_{ON} that set $B = 0$ form a straight line in the phase diagrams (black lines in Fig. 1b). Note that close to $B = 0$, we have high values of the multicellular entropy (from Maire and Youk, *Cell Systems* (2015)). This indicates that most of the microstates are stable.

To be more concrete, let us first analyze the interactions between pairs of cells. The cellular automaton updates cell-i's state by coupling the signal concentration Y_i on it with its state X_i at the next time step. By equation S9, we see that if X_i's are initially independent of each other, then we have

$$\text{Cov}(\vec{X}) = \sigma_p^2 \mathbb{I} \tag{S56}$$

where $\mathbb{I}$ is the identity matrix. Moreover, we have

$$\text{Cov}(\vec{Y}) = (C_{ON} - 1)^2 \sigma_p^2 M^T M \tag{S57}$$

By the definition of M (equation (S10)), we see that as the distance between two cells get closer to each other, the more correlated their states become. Since the cells' states are updated at every time step with the same matrix M, we conclude that $\sum_i \sum_{j \neq i} f(r_{ij}) X_i X_j$ monotonically increases over time. This in turn causes H (and thus h) to monotonically decrease over time. This is another way of stating what we will show in the next section: the Θ defined in Eq. S14, monotonically increases over time.

We now need to analyze the term in H that depends on the signal field B. The phase diagram can be divided into regions in which $B > 0$ and regions in which $B < 0$. Separating the two regions is the straight line along which $B = 0$. In the region in which $B > 0$, activate phase resides as well as the autonomy phase (for weak interactions) or the activate-deactivate phase (for strong interactions). In the activate phase, we can see that $B \sum_i X_i$ increases and H decreases over time. In the region in which $B < 0$, deactivate phase resides as well as the autonomy phase (if weak interaction) or the activate-deactivate phase (if strong interaction). In the deactivate phase, it follows that H decreases over time. So we are now left with the autonomy phase and the activate-deactivate phase (both near $B = 0$). In the autonomy phase, $\Delta H = 0$ because every microstate is a steady state.

We have so far shown that the H (and thus h) is a non-increasing function over time in all phases except in the activate-deactivate phase. Let us now show that the h is also a non-increasing function over time in the activate-deactivate phase. To do so, we first rewrite h in terms of the spatial index I and the fraction p of cells that are ON. To do so, we first write Y_i in terms of X_i:

$$Y_i = \frac{(C_{ON}-1)}{2}(X_i+1)+1+\sum_{j\neq i}\left[\frac{(C_{ON}-1)}{2}(X_j+1)+1\right]f(r_{ij}) \tag{S58}$$

where $f(r_{ij})$ is the term for the cell pair (i,j) in the interaction strength function. Using this equation and noting that $\sum_i X_i = (2p-1)N$ and $\sum_{j\neq i} f(r_{ij}) = f_N$, we have

$$H = -\frac{N(C_{ON}-1)}{2} - \frac{N(C_{ON}+1)}{2}(2p-1)(1+f_N) - \frac{(C_{ON}-1)}{2}\sum_i\sum_{j\neq i} f(r_{ij})X_iX_j \tag{S59}$$

It then follows that

$$h = -\frac{(C_{ON}-1)}{2}\left(1+4f_Np(1-p)I+(2p-1)^2f_N\right) - (2p-1)\left[\frac{(C_{ON}+1)}{2}(1+f_N)-K\right] \tag{S60}$$

Now note that in the activate-deactivate phase, B takes on both positive and negative values. However, the Θ monotonically increases over time (as we shown in Section S3). Thus from equation S60, we have

$$\Delta h \leq -2(B+2f_N(2p-1))\Delta p \tag{S61}$$

which is less or equal to zero if

$$\Delta p \geq 0 \quad \text{if } p \geq \frac{1}{2} - \frac{B}{4f_N} \tag{S62a}$$

$$\Delta p \leq 0 \quad \text{if } p \leq \frac{1}{2} - \frac{B}{4f_N} \tag{S62b}$$

In Fig. S3, we see that indeed the condition S62 is satisfied and the pseudo-energy monotonically decreases in the activate-deactivate phase. Moreover, note that close to the line defined by $p = \frac{1}{2} - \frac{B}{4f_N}$, which separates the activation-dominant regions from the deactivation-dominant regions in the activate-deactivate phase, we have mostly autonomy - cells do not switch their states here. Therefore, for $B \approx 0$, we have autonomous behaviours with $p \approx \frac{1}{2}$ and, consequently, the secrete-and-sense cells obtain a higher entropy.

Putting everything together, we see that indeed the H, and thus the h, monotonically decreases in all phases as the cellular automaton proceeds.

S5 Derivation of the trapping probability - $P_{eq}(p, I)$

The concentration Y_i sensed by cell-i is:

$$Y_i = Y_i^{\text{self}} + Y_i^{\text{nei}} \tag{S63}$$

where Y_i^{self} is the self-contribution (i.e., signal secreted by cell-i itself) and Y_i^{nei} is the contribution from all other cells. Specifically, they are

$$Y_i^{\text{self}} = (C_{ON}-1)\,X_i + 1 \tag{S64a}$$

$$Y_i^{\text{nei}} = \sum_{j\neq i}\left[(C_{ON}-1)\,X_j+1\right]\frac{e^{R-r_{ij}}}{r_{ij}}\sinh(R) \tag{S64b}$$

The probability that an ON-cell remains ON in the next time step is the same as the probability $P_{ON\to ON}$ that the signal concentration on an ON-cell is larger than the threshold concentration K:

$$P_{ON\to ON} = P\left(Y_i > K \middle| X_i = 1\right) = P\left(Y_i^{\text{nei}} > K - C_{ON}\middle| X_i = 1\right) \tag{S65}$$

Similarly defining $P_{OFF\to OFF}$ as the probability that an OFF cell senses a concentration of the signal that is lower than K, we have

$$P_{OFF\to OFF} = P\left(Y_i < K \middle| X_i = 0\right) = P\left(Y_i^{\text{nei}} < K-1 \middle| X_i = 0\right) \tag{S66}$$

We will show below that $P_{ON\to ON}$ and $P_{OFF\to OFF}$ are expressible in terms of p and I. If we randomly pick a microstate out of a "box" that belongs to a macrostate $(p,\, I)$, the probability that the microstate is an equilibrium state is given by the **trapping probability** $P_{eq}(p, I)$, where

$$P_{eq}(p, I) = \left(P_{ON\to ON}\right)^n \left(P_{OFF\to OFF}\right)^{N-n} \tag{S67}$$

Since we do not know exactly where each ON- and OFF-cell is but only know that there is a total of n ON-cells, we treat X_i for all i as a random variable. Accordingly, Y_i^{nei} is also a random variable. Furthermore, by placing the cells in the lattice in a completely random fashion, Y_i^{nei} does not depend on the state of cell-i, X_i. Thus

$$P_{ON\to ON} = P\left(Y_i^{\text{nei}} > K - C_{ON}\right) \tag{S68a}$$
$$P_{OFF\to OFF} = P\left(Y_i^{\text{nei}} < K - 1\right) \tag{S68b}$$

We assume that X_i follows a binomial distribution with a probability $p = n/N$. Then the mean of the X_i distribution is p and the variance is $(1-p)p$. For a large N, the Central limit theorem dictates that $\langle X_i\rangle$ is normally distributed:

$$\langle X_i\rangle \sim \mathcal{N}\left(p, p(1-p)\right) \tag{S69}$$

where $\mathcal{N}\left(\mu, \sigma^2\right)$ is the normal distribution with mean μ and variance σ^2. To find how Y_i^{nei} is distributed, we use equation S64b. Since each cell's position is fixed, Y_i^{nei} is linear in X_i and is thus also normally distributed. This means that we only need to compute the mean and the variance of Y_i^{nei}, which depend on both p and the spatial index I. Because I is related to whether a cell has neighbours that are similar or different from itself, the sensed concentration for an OFF-cell will be different from for an ON-cell within the same configuration whenever $I \neq 0$. For an OFF-cell, we write $Y_{i=OFF}^{\text{nei}} \sim \mathcal{N}\left(\mu_{OFF}, \sigma_{OFF}\right)$, whereas for an ON-cell we have $Y_{i=ON}^{\text{nei}} \sim \mathcal{N}\left(\mu_{ON}, \sigma_{ON}\right)$.

To calculate the means and variances, we first change notation and define $\tilde{X} = 2X - 1$, so that $\tilde{X} \in \{-1, 1\}$. Then we can write

$$Y_i^{\text{nei}} = \left(\frac{C_{ON}+1}{2}\right) f_N + \left(\frac{C_{ON}-1}{2}\right) \sum_{i\neq j} f(r_{ij})\tilde{X}_j \tag{S70}$$

Taking the average of above, we have

$$\mu_{ON} = \left(\frac{C_{ON}+1}{2}\right) f_N + \left(\frac{C_{ON}-1}{2}\right) \langle \sum_{i\neq j} f(r_{ij})\tilde{X}_j | i = ON\rangle \tag{S71a}$$
$$\mu_{OFF} = \left(\frac{C_{ON}+1}{2}\right) f_N + \left(\frac{C_{ON}-1}{2}\right) \langle \sum_{i\neq j} f(r_{ij})\tilde{X}_j | i = OFF\rangle \tag{S71b}$$

Note that we can write the expression for Θ (Eq. S14) as

$$\Theta = p\langle \sum_{i\neq j} f(r_{ij})\tilde{X}_j | i = ON\rangle - (1-p)\langle \sum_{i\neq j} f(r_{ij})\tilde{X}_j | i = OFF\rangle \tag{S72}$$

At the same time, using Bayes' theorem we have

$$\langle \sum_{i\neq j} f(r_{ij})\tilde{X}_j\rangle = (2p-1) f_N = p\langle \sum_{i\neq j} f(r_{ij})\tilde{X}_j | i = ON\rangle + (1-p)\langle \sum_{i\neq j} f(r_{ij})\tilde{X}_j | i = OFF\rangle \tag{S73}$$

Combining S72 and S73 allows us to solve for $\langle \sum_{i\neq j} f(r_{ij})\tilde{X}_j | i = ON\rangle$ and $\langle \sum_{i\neq j} f(r_{ij})\tilde{X}_j | i = OFF\rangle$. Combined with S71 we obtain

$$\mu_{ON} = f_N\left[C_{ON}p + 1 - p + (C_{ON}-1)(1-p)I\right] \tag{S74a}$$
$$\mu_{OFF} = f_N\left[C_{ON}p + 1 - p - (C_{ON}-1)pI\right] \tag{S74b}$$

For the variance of the sensed concentration of the signal, we change back to the original notation with $X_i \in \{0, 1\}$. From a mean-field approximation we then obtain

$$\langle Y_i^{\text{nei}} \rangle = \sum_{j \neq i} \left[(C_{ON} - 1) \langle X_j \rangle + 1 \right] \frac{e^{R - r_{ij}}}{r_{ij}} \sinh(R) = \left[(C_{ON} - 1)\, p + 1 \right] f_N(a_0) \equiv \mu_p \tag{S75}$$

Moreover, we have

$$\langle \left(Y_i^{\text{nei}} \right)^2 \rangle = \sum_{j \neq i} (C_{ON} - 1)^2 \langle X_j^2 \rangle \frac{e^{2(R - r_{ij})}}{r_{ij}^2} \sinh^2(R) = (C_{ON} - 1)^2\, p(1-p) g_N(a_0) \equiv \sigma_p^2 \tag{S76}$$

where we have defined the function

$$g_N(a_0) \equiv \sum_{j \neq i} \frac{e^{2(R - r_{ij})}}{r_{ij}^2} \sinh^2(R) \tag{S77}$$

From this, we obtain

$$\sigma_{ON} = \sigma_{OFF} = (C_{ON} - 1) \sqrt{g_N p (1-p)} \tag{S78}$$

Combining above results, we finally have

$$P_{ON \to ON} = 1 - D(K - C_{ON}; \mu_{ON}, \sigma_{ON}) = \frac{1}{2} \left[1 - \text{erf}\left(\frac{K - C_{ON} - \mu_{ON}}{\sqrt{2} \sigma_{ON}} \right) \right] \tag{S79a}$$

$$P_{OFF \to OFF} = D(K - 1; \mu_{OFF}, \sigma_{OFF}) = \frac{1}{2} \left[1 + \text{erf}\left(\frac{K - 1 - \mu_{OFF}}{\sqrt{2} \sigma_{OFF}} \right) \right] \tag{S79b}$$

where $D(x; \mu, \sigma)$ is the cumulative distribution function of the Gaussian with mean μ (equation S74) and standard deviation σ (equation S78) while $\text{erf}(x)$ is the error function.

S6 Equation of motion derived from the pseudo-energy

In this section we derive the equation of motion (Eq. 4 in the main text), determine the values of the new variables in this equation of motion and discuss on a technical level the validity of the approach. A more colloquial discussion is included in the main text.

From observations, we see that the simulated trajectories follow paths whose directions tend to point in the direction of fastest descent of the pseudo-energy (Fig. 4). This motivates us to construct an equation that utilizes the direction of fastest descent. The gradient of the pseudo-energy is given by $\vec{\nabla} h = (\frac{\partial h}{\partial p}, \frac{\partial h}{\partial I})$, with

$$\begin{aligned} \frac{\partial h}{\partial p} &= -(C_{ON} - 1) 2 f_N (1 - I)(2p - 1) - (C_{ON} + 1)(f_N + 1) + 2K, \\ \frac{\partial h}{\partial I} &= -2 f_N (C_{ON} - 1) p (1 - p). \end{aligned} \tag{S80}$$

Note that the above expression implies that there are no local minima of h which are not on the boundary of the (p, I) phase space. This follows from the fact that the gradient must vanish at a local minimum, and the only points at which $\frac{\partial h}{\partial I}$ vanishes are $(p, I) = (0, 0)$ and $(p, I) = (1, 0)$ (taking into account the fact that $p = 0$ and $p = 1$ have only one microstate with $I = 0$, see Section S2). Hence for $0 < p < 1$ there can be no local minima. Therefore, the trapped configurations alluded to in the main text cannot be directly related to the minima of the pseudo-energy.
Recall that the direction of steepest descent at any point (p, I) is given by the negative of the gradient, $-\vec{\nabla} h$. As a first attempt, we can therefore try as phenomenological equations

$$\begin{aligned} \frac{\partial p}{\partial t} &= -\frac{\partial h}{\partial p}, \\ \frac{\partial I}{\partial t} &= -\frac{\partial h}{\partial I}. \end{aligned} \tag{S81}$$

While in some cases the streamlines produced by this vector field closely approach the automaton simulations, Eq. S81 misses out an important aspect of the macrostate-level dynamics. The dynamics it produces is deterministic, providing only one possible trajectory for a given starting macrostate (p_0, I_0). This ignores the fact that the macrostate-level description is degenerate - A macrostate (p, I) usually has many microstates, which could follow multiple non-identical trajectories.

Hence we need to introduce noise terms to represent our ignorance of the microstates. We choose to add white noise, constructing a Langevin equation where the (negative of the) gradient represents the drift term and the Brownian motion corresponds to the variability between trajectories of different initial microstates. The next caveat is that the cellular automaton operates in discrete time, where a Langevin equation consisting of S81 with added noise terms would naturally be described in continuous time. To better assess the compatibility of the Langevin equation with our discrete time cellular automaton, we need to modify it into a discrete time equation whose time steps reflect average changes in the automaton.

To do this, we first introduce a step size δ, which is a scaling factor that controls how far along the negative of the gradient the system should travel in one time step. Our discrete-time system then becomes

$$\begin{aligned}\Delta p &= -\frac{\partial h}{\partial p}\delta + \eta_p,\\ \Delta I &= -\frac{\partial h}{\partial I}\delta + \eta_I.\end{aligned} \tag{S82}$$

Here we have introduced the noise as Gaussian variables $\eta_p \sim \mathcal{N}(0, \sigma_p), \eta_I \sim \mathcal{N}(0, \sigma_I)$. Next, we will derive expressions for these parameters based on the microstate-level details of the system.

S6.1 Mean-field calculation of Δp, used for obtaining δ

In this section we provide a calculation of Δp based on the switching probabilities $P_{ON\to ON}$ and $P_{ON\to ON}$ used in section S5. By comparing the result with Eq. S82 we can fix the value of δ, as we will show in the next section.

Recall that Δp is the amount of change in p at time step t. Using the probabilities calculated in the section S5, we can calculate by how much p changes at time t: $\Delta p_t = p_{t+1} - p_t$. We will use this to obtain a constant scale factor δ that rescales the gradient of the pseudo-energy in the equation of motion (details in Section S6). We assume that all ON-cells have a binomial chance of transitioning to an OFF state with probability $1 - P_{ON\to ON}$. Therefore, if at time t we have n_t ON-cells, the probability that y_- ON-cells will switch OFF in the next time step is

$$P(y_-; n, 1 - P_{ON\to ON}) = P_{ON\to ON}^{n-y_-}(1 - P_{ON\to ON})^{y_-}\binom{n}{y_-} \tag{S83}$$

Similarly, the probability that y_+ OFF-cells will switch ON in the next time step is

$$P(y_+; n, 1 - P_{OFF\to OFF}) = P_{OFF\to OFF}^{N-n-y_+}(1 - P_{OFF\to OFF})^{y_+}\binom{N-n}{y_+} \tag{S84}$$

Note that this is the same reasoning that we used for calculating the transition matrix in the previous section. We are now interested in the mean and the variance of Δp_t. Note that

$$N\Delta p_t = y_+ - y_- \tag{S85}$$

The mean of a binomial distribution with N draws and probability p is Np. Hence, taking the average of equation S85, we obtain the average of Δp_t:

$$\langle \Delta p_t \rangle \equiv E(p_+) - E(p_-) = (1-p)(1 - P_{OFF\to OFF}) - p(1 - P_{ON\to ON}) \tag{S86}$$

To calculate the variance of Δp_t, we assume that we can approximate the distributions S83 and S84 as being independent Gaussians. This assumption is certainly true when n and $N-n$ are both sufficiently large. With this assumption, we obtain the following simplified result for the variance:

$$\mathrm{Var}\,(\Delta p_t) \approx \mathrm{Var}\,(p_+) + \mathrm{Var}\,(p_-) = \frac{1}{N}\left[(1-p)(1 - P_{OFF\to OFF})P_{OFF\to OFF} + p(1 - P_{ON\to ON})P_{ON\to ON}\right] \tag{S87}$$

Note that in the thermodynamic limit ($N \to \infty$), the variance of Δp_t goes to zero as expected.

S6.2 Parameters of the equation of motion

We will use the results derived above to fix δ. Recall that the probabilities $P_{ON\to ON}$ (Eq. S65) and $P_{OFF\to OFF}$ (Eq. S66) are functions of p and I, so $\langle\Delta p\rangle$ depends on both p and I. This suggests a way of fixing $\delta = \tilde{\delta}(p)$ defined through

$$\langle\Delta p\rangle = -\frac{\partial h}{\partial p}\tilde{\delta}(p). \tag{S88}$$

In this way, the equation of motion would always predict Δp to be equal to $\langle\Delta p\rangle$ as given in S86. However, the quantity $\tilde{\delta}(p)$ depends on p through $\langle\Delta p\rangle$ and $\frac{\partial h}{\partial p}$ which is inconsistent with how to arrived at S82. To obtain a constant scaling factor, we have to average this quantity over a suitable weight function on (p, I) space. We choose to average this quantity over p with as weight the fraction of states with n ON cells or $p = n/N$,

$$f_p = \frac{1}{2^N}\binom{N}{n}. \tag{S89}$$

Since I enters the equations only through $\frac{\partial h}{\partial p}$, which depends linearly on I, we make the approximation that $I = 0$. This is justified by calculations in which we find that the density of states (i.e. the number of microstates corresponding to a macrostate (p, I)) is highest around $I \approx 0$ for each value of p (not shown). Thus we obtain δ through a doubling averaging procedure as

$$\delta = \sum_{n=0}^{N} f_p\,\tilde{\delta}(p) = -\sum_{n=0}^{N} f_p\langle\Delta p\rangle\left(\frac{\partial h}{\partial p}\right)^{-1}. \tag{S90}$$

More explicitly,

$$\delta = \sum_{n=0}^{N}\frac{1}{2^N}\binom{N}{n}\frac{(1-p)(1-P_{OFF\to OFF}) - p(1-P_{ON\to ON})}{(C_{ON}-1)2f_N(2p-1) + (C_{ON}+1)(f_N+1) - 2K}. \tag{S91}$$

Here, we implicitly also take $I = 0$ in the expressions for $P_{ON\to ON}$ and $P_{OFF\to OFF}$.

To estimate the noise, we use S86, but now derive

$$\begin{aligned} N^2\mathrm{Var}(\Delta p) &= \mathrm{Var}(y_+) + \mathrm{Var}(y_-) - 2\,\mathrm{Cov}(y_+, y_-) \\ &= \mathrm{Var}(y_+) + \mathrm{Var}(y_-) \\ &= N(1-p)(1-P_{OFF\to OFF})P_{OFF\to OFF} \\ &\quad - Np(1-P_{ON\to ON})P_{ON\to ON}. \end{aligned} \tag{S92}$$

The first equality follows from the independence of y_+ and y_-, and the second follows from the properties of the binomial distribution. As for δ we first define a p-dependent (or n-dependent) standard deviation

$$\tilde{\sigma_p}(n) = \sqrt{(1-p)(1-P_{OFF\to OFF})P_{OFF\to OFF} - p(1-P_{ON\to ON})P_{ON\to ON}}. \tag{S93}$$

Hence we define the noise in Δp as

$$\sigma_p = \sum_{n=0}^{N} f_p\tilde{\sigma_p}(n). \tag{S94}$$

To obtain the first two moments of ΔI, we note that in the absence of noise, any change in I is related to the change of p through the gradient (Eq. S82), namely through

$$\Delta I = \frac{\partial h}{\partial I}\left(\frac{\partial h}{\partial p}\right)^{-1}\Delta p. \tag{S95}$$

We now assume that the same relation holds for the first two moments of ΔI, giving

$$\begin{aligned} \langle\Delta I\rangle &= \frac{\partial h}{\partial I}\left(\frac{\partial h}{\partial p}\right)^{-1}\langle\Delta p\rangle, \\ \sigma_I &= \frac{\partial h}{\partial I}\left(\frac{\partial h}{\partial p}\right)^{-1}\sigma_p, \end{aligned} \tag{S96}$$

S6.3 Stopping condition

Equation S82 alone cannot predict where the trajectories will end. If we do not impose any conditions, the trajectories would always escape from the allowed phase space or end at the edge, as we have seen that there can be no points with $0 < p < 1$ where the gradient vanishes. To fix this problem and predict terminal macrostates for our system, we set up two more rules for the evolution of S82. First, let the system terminate at (p, I) with probability $P_{eq}(p, I)$, the trapping probability $P_{eq}(p, I)$ we derived in Section S5. This is done through a Monte Carlo step, in which we draw a random number and compare it with $P_{eq}(p, I)$ to decide whether to terminate the simulation.

Second, we add an additional rule near the boundaries of the phase space. As the particle trajectories have a tendency to cross $p = 0$ or $p = 1$ at values of $I \neq 0$, we need to impose an additional stopping condition to prevent the particle from leaving the phase space (i.e., $p > 1$ and $p < 0$). Recall that for $p = 0$ and $p = 1$ we only have one microstate with $I = 0$. Therefore, we set up the additional rule that $(p, I) \to (0, 0)$ and $(p, I) \to (1, 0)$ when the system attempts to exit the phase space across $p = 0$ or $p = 1$ respectively.

S6.4 Particle trajectories from the gradient field of the pseudo-energy and P_{eq}

Given the equation of motion and P_{eq}, we can predict the particle trajectories and compare them with the particle trajectories produced by the cellular automaton. We find that for all the different behavioural phases, the equation of motion approximates the trajectories well and generally predicts the correct final (resting) configurations (Figs. S4, S5 and S6). A more detailed discussion of these results is given in the main text.

Note that we can clearly identify a region of low P_{eq} (blue) and a region of high P_{eq} (yellow) with a relatively sharp transition between them. Furthermore, the cellular automata terminate mostly in regions where P_{eq} is high. These two features imply that that using only P_{eq}, we can predict in which regions in (p, I) the particles will likely come to a rest, if it ever reached the region. Also, it means that there is a graphical way to estimate the particle trajectories and their stopping points in the (p, I)-space. First, we plot the vector field and P_{eq} together (Figs. 4 and S4-S5). From the directions of the vector field, we can estimate how the particle will move. By tracing out these trajectories until the particles reach a region where the P_{eq} is high, we can get an estimate of the final (p, I) of the trajectory. As seen in Figs. S4-S5, this gives a good estimate of the direction and endpoints of the trajectories. The match between the particle trajectories dictated by the equation of motion and those produced by the cellular automaton depends on the parameters (i.e., C_{ON}, K, and f_N), but in general the overall direction and endpoints match well.

S6.5 Why the gradient approach works: the allowed range of directions

Apart from observing that the particles seem to move in the direction of steepest descent of h, we can make a more precise mathematical argument as for why $-\vec{\nabla}h$ is a good estimate for the particle's direction of the motion. The argument that we will give here will also show that the range of allowed directions is much larger (spanning an arc of π radians or half a circle). Whether the trajectories are likely to match with gradient vector field or not in part depends on how its direction relates to this range of allowed directions. In particular, whenever the gradient is (close to) horizontal (i.e., zero degrees) or vertical (i.e., $\pi/2$ raidans) in the (p, I) space, significant deviations from the direction of steepest descent are possible.

The fact that the pseudo-energy is a Lyapunov function means that the system can only move in a direction for which the pseudo-energy decreases. It cannot move in the direction of the (positive of the) gradient $\vec{\nabla}h$ and by continuity also not in a direction close to it. To be precise, define $\vec{v} = (\cos\theta, \sin\theta)$ as a unit vector and define θ as the angle it makes with the gradient $\vec{\nabla}h$. Recall that the system does not have any local minima as shown earlier, so the gradient cannot vanish. Therefore θ is well-defined. Define

$$\Delta h(\theta) = \vec{\nabla}h \cdot \vec{v}(\theta) \tag{S97}$$

It follows that $\Delta h(0) > 0$ and $\Delta h(\pi) < 0$, as the gradient and negative of the gradient point in directions of steepest ascent and descent respectively. By continuity, there exist $0 < \theta_1 < \pi$ and $\pi < \theta_2 < 2\pi$ for which $\Delta h(\theta_1) = 0$ and $\Delta h(\theta_2) = 0$ (Intermediate Value Theorem). Hence we can define an interval $I_\theta \equiv [\theta_1, \theta_2]$ that

gives the range of directions in which h decreases, i.e. for all $\theta \in I_\theta$, we have $\Delta h(\theta) \leq 0$. From $\Delta h(\theta) = 0$, we see that θ_1 and θ_2 are solutions to

$$\tan\theta = -\frac{\partial h}{\partial p}\left(\frac{\partial h}{\partial I}\right)^{-1} \tag{S98}$$

This has an exact solution on $S^1 = \{0 \leq \theta \leq 2\pi | 0 \equiv 2\pi\}$ with $\theta_2 = \theta_1 + \pi$. Therefore, $|I_\theta| = \pi$. Conversely, the minimum and maximum of $\Delta h(\theta)$ are defined through $\frac{d\Delta h(\theta)}{d\theta} = 0$, for which the solution is $\tan\theta = \frac{\partial h}{\partial p}\left(\frac{\partial h}{\partial I}\right)^{-1}$. From the properties of the tangent function, one can check that the solutions to $\tan x = c$ and $\tan x = -c$ are close to each other whenever $|c|$ is either very small or very large. Note that the angles are defined on a circle, so distances are measured by taking the solutions modulo 2π. This implies that the minimum is close to the bounds of I_θ whenever $\frac{\partial h}{\partial p}\left(\frac{\partial h}{\partial I}\right)^{-1}$ goes to 0 or ∞. This can only happen if either $\frac{\partial h}{\partial p} \to 0$ or $\frac{\partial h}{\partial I} \to 0$.

S6.6 Limitations of the gradient approach

The argument above shows that the negative of the gradient gives a direction of the particle's motion indication and represents a first-order approximation. However, the range of directions in which the system is in principle able to move (given its macrostate) is in fact much wider - the unit vectors of the allowed directions lie on a half circle which contains $-\hat{\nabla}h$ (unit vector pointing in direction of $-\vec{\nabla}h$). Whether the trajectories will seem close to the negative of the gradient depends on the position of $-\hat{\nabla}h$ on this half circle. If $-\hat{\nabla}h$ points at the middle of this 'allowed arc', then the trajectories can deviate at most a right angle from $-\hat{\nabla}h$. However, if $-\hat{\nabla}h$ is in a direction close to one of the edges, then deviations can in principle approach a limiting value of 180 degrees. We have shown in the previous section that the latter occurs only if the vector field points close to vertical or horizontal. Indeed, a closer look at the trajectories of Figs. S4 - S5 reveals that significant deviations from the automaton trajectories are almost exclusively found in cases where the vector field is close to horizontal or vertical. This is apparent in all of the weak interaction pictures (Fig. S4), but also in the region in which the horizontal component of the vector field changes sign in the strong interaction regime (Fig. S5).

S7 Extension to stochastic secretion-and-sensing: A proof of principle

In this section, we obtain a statistical dynamics of secrete-and-sense cells with a stochastic secretion and sensing. We will simulate these cells through 'noisy cellular automata'. By extending our framework for deterministic cellular automaton, **we show in this section that molecular and cellular noise can promote generation of spatial configurations that are much more ordered than the configurations obtained from the deterministic cellular automaton.**

S7.1 Incorporating stochastic secreting-and-sensing into secrete-and-sense cells

A noise (or the cell's "error") in secreting and the noise in sensing would be reflected as fluctuations in the value of C_{ON} and K respectively. But instead of running the cellular automaton with the values of C_{ON} and K both varying from cell to cell on the same lattice, we adopt a simpler procedure here. Note that the variability in the value of C_{ON} among cells on the same lattice would mean that there would be fluctuations in the value of the signal concentrations Y_i's on each cell. But since it is the difference between Y_i and K that determines the state of cell-i, the secrete-and-sense cells would only need to care about the fluctuation in $Y_i - K$. We can introduce fluctuations in $Y_i - K$ by calculating Y_i deterministically while introducing random variations in K from one cell to another [2]. Hence, in each time step of our stochastic cellular automata, each cell in the lattice has a different activation threshold $K_{\text{i, noise}}$ which also varies over time:

$$K_{i,\text{noise}} = K + \delta K_i \tag{S99}$$

[2]The only difference between introducing noise only in K and in both K and C_{ON} is that in the latter case, we would have a higher noise when p is higher. However, the basal secretion rate (i.e. secretion rate of an OFF-cell) would also fluctuate and we would thus have to introduce noise in C_{OFF}, which we previously set to 1, as well. We opted for the simpler implementation in which we add noise only to K.

where the random noise term δK_i is assumed to be distributed according to a Gaussian $\mathcal{N}$ with a mean of zero and a standard deviation α:

$$\delta K_i \sim \mathcal{N}(0, \alpha^2) \tag{S100}$$

We assume that the noise δK_i is normally distributed. Note that δK_i is in units of the basal level concentration and that α has to be compared to the values of K and C_{ON} to determine if it is "large" or "small". To make these ideas concrete, we define **noise strength** $\xi = \alpha/K$, which is the fractional error in the activation threshold.

S7.2 Noise strength required to perturb the secrete-and-sense cells

We compute the probability that noise will change the fate of a cell in the cellular automaton. For simplicity, we ignore the spatial index (i.e. $I = 0$) and assume that the mean-field approximation - assuming that ON-cells are randomly distributed over the lattice - is sufficient for calculating the signal concentration on a cell due to all the other cells. Then using equation S75, an ON-cell senses

$$\langle Y_{i=ON} \rangle = C_{ON} + f_N \left(pC_{ON} + 1 - p \right) \tag{S101}$$

with variance σ_p given by equation S78. Therefore, for an ON-cell, we have that the variable $Y_i - K$ has mean

$$\langle Y_{i=ON} - K \rangle = C_{ON} + f_N \left(pC_{ON} + 1 - p \right) - K \tag{S102}$$

and variance

$$\mathrm{Var} \left(Y_{i=ON} - K \right) = \sigma_p^2 + \alpha^2 \tag{S103}$$

where we used the fact that σ_p and α are uncorrelated. Noise is relevant to the secrete-and-sense cells (i.e. produces dynamics distinct from that of the deterministic cellular automaton) if $\alpha \sim \sigma_p$ and

$$\alpha \sim |\langle Y_{i=ON} - K \rangle| \tag{S104}$$

For instance if $\alpha >> \sigma_p$ [3] and $\alpha = |\langle Y_{i=ON} - K \rangle|$ then due the fact that we are using a Gaussian noise (i.e. $\delta K_i \sim \mathcal{N}(0, \alpha^2)$), there is a chance of around 30% that the noise will cause a cell to deviate from its deterministic trajectory in phase space. However, if α is $1/3$ of this value, the chance that the noise changes the deterministic dynamics of ON-cells is reduced to 0.3%. We can analyse OFF-cells in a similar manner by noting that

$$\langle Y_{i=OFF} - K \rangle = 1 + f_N \left(pC_{ON} + 1 - p \right) - K \tag{S105}$$

and using the same variance as in equation S103. This in turn defines another condition for α:

$$\alpha \sim |\langle Y_{i=OFF} - K \rangle| \tag{S106}$$

Note that equations S104 and S106 depend on p. Since we are concerned with dynamics of the macrostates, we can use the fact that the fluctuations due to noise would scale as $\sqrt{N}$. Thus, the minimum α required for noise to significantly alter the deterministic dynamics (i.e., the dynamics of the deterministic cellular automaton) is

$$\alpha_{\min} = \frac{1}{\sqrt{N}} \min \left(|\langle Y_{i=ON} - K \rangle|, |\langle Y_{i=OFF} - K \rangle| \right) \tag{S107}$$

We find that when the noisy secrete-and-sense cells operate with a weak interaction strength and in the autonomy phase, the minimum required noise strength is typically low. This makes an intuitive sense because when the interaction strength is low, a cell's state is only weakly influenced by the rest of the cells thus even low amounts of noise is sufficient to change each autonomous cell's state (i.e. noise does not have to fight against the influence of the rest of the population). Above equation also says that even when the noise has a very low strength, of about 1%, it can drastically affect the deterministic dynamics. This reinforces the notion that noise is crucial in understanding the dynamics of tissues, biofilms, and other multicellular systems, in which noise is typically higher than the calculated minimum noise strength. As a final remark in this section, we note that even when the secrete-and-sense cells operates have a noise strength that is lower

[3] This is reasonable since $\sigma_p = 0$ when all cells are in the same state.

than the minimum noise strength, the Gaussian nature of the fluctuation implies that there is a (extremely) small probability that a cell in the population will have its dynamics noticeably changed by the very weak noise. However, this would require a very long time (potentially indefinite) to occur, perhaps spanning longer than the lifetime of the organism.

S7.3 Perturbing all ON and all OFF configurations with noise: a case study

To illustrate how noise perturbs the deterministic dynamics of the secrete-and-sense cells, let us consider two spatial patterns that are stable without noise: (1) "all-OFF" configuration in which all cells are OFF and (2) the "all-ON" configuration in which all cells are ON.

Let us start with the all-OFF configuration. Introducing noise into the cellular automaton would cause the number of ON-cells to fluctuate above zero over time. We have $Y_i = 1 + f_N$ for all cells. Therefore, the mean fraction $\langle p \rangle$ of cells that are ON given a noise strength α is

$$\langle p \rangle = D\left(0; K - 1 - f_N, \alpha\right) \tag{S108}$$

where the function $D\left(0; K - 1 - f_N, \alpha\right)$ is the cumulative distribution function of a Gaussian with mean $K - 1 - f_N$ and a standard deviation α. Note that $\langle p \rangle$ is determined by the probability that a single cell will turn ON due to noise. For the all-ON configuration, we use a similar logic to obtain the average fraction $\langle p \rangle$ of cells that are OFF

$$\langle p \rangle = 1 - D\left(0; K - C_{ON}(1 + f_N), \alpha\right) \tag{S109}$$

To compare these estimates to the results of the noisy cellular automaton, as a case study, we chose the parameters so that the secrete-and-sense cells operated in the activate-deactivate phase. In this phase, all cells being ON and all cells being OFF are both steady states of the deterministic secrete-and-sense cells. Which one of two configurations is realized by the secrete-and-sense cells depends on the initial values of (p, I). To test our estimates, we start the noisy cellular automaton with either all cells ON or all cells OFF. We ran many noisy cellular automata, each with different noise strengths. Comparing our estimates of $\langle p \rangle$ with the $\langle p \rangle$ obtained from the noisy cellular automata (Fig. S8), we found that our estimates more closely match the $\langle p \rangle$ obtained from the noisy cellular automaton when the noise strength is low than when it is high. Moreover, we found that when the noise strength is high, our formulas (equations S108 and S109) underestimate $\langle p \rangle$. Yet in many cases with strong noise, the two values are still quite close to each other (Fig. S8). The reason is that as more cells turn ON, it becomes more difficult for the other cells to change their states in the next time step. This is especially true for cells that are in the neighbourhood of an activated (or a deactivated) cell.

S7.4 Temporal evolution of the pseudo-energy due to noise

A state that is stable without noise can become unstable after we introduce noise. But fluctuations do not necessarily occur around a state that is a steady-state of the deterministic cellular automaton. For example, in the activate-deactivate phase, all particle trajectories may lead to all cells being ON when no noise is present. But when noise is present, we find that the same initial macrostate can evolve towards a final spatial configuration in which all cells are OFF. This occurs because of the population effect mentioned in the previous section. Noise of sufficiently high strength can drive the spatial configuration to one of two configurations, both of which drive the particle that represents the spatial configuration to a global minimum of the pseudo-energy landscape, where either all cells are ON or all cells are OFF. If the cellular automaton runs for a sufficiently long time with a sufficiently strong noise, then a metastable spatial pattern can be driven into one of these two configurations. After reaching either the all-ON or the all-OFF spatial configurations, the cellular lattice will fluctuate around these two configurations (i.e., the particle that represents the cellular lattice diffuses around the corresponding locations on the pseudo-energy landscape). As we have seen in the deterministic cellular automaton, cellular lattice's spatial organization increases because doing so makes the neighbouring cells help each other in keeping their states. The same happens here. But now with noise, any possible steady state spatial configuration is constantly perturbed by the noise. The most stable spatial configurations are the ones in which the cells reinforce each others' states through cell-cell interactions. Minimizing the pseudo-energy means that the value $|Y_i - K|$ is maximized for every cell. The resulting spatial configuration, in turn, minimizes the effect of noise as discussed in section S7.

S7.5 Spatial ordering due to noise: Noise can stabilize and create more ordered spatial configurations through slow (glass-like) dynamics that destroy the insulating phases while promoting signal conduction among cells

A primary feature of noisy secrete-and-sense cells' dynamics is that noise of a sufficient strength can reinforce (effectively strengthen) cell-cell interactions and as a result, the cellular lattice tends to evolve to a spatial configuration in which all cells are either ON or OFF. Accordingly, the particle (cellular lattice) would roll down the pseudo-energy landscape and eventually reach the minimum. But if the noise strength is not too high, this process can be very slow, involving the particle (cellular lattice) getting stuck at multiple metastable states (metastable spatial configurations) or being stuck in one metastable state and taking a very long time to escape it. In this section, **we will show that (i) clusters of ON- and OFF-cells occur more frequently with noise than without noise, and that (ii) these clusters can be stable for a long time despite being constantly bombarded by noise.**

S7.5-a. Noise destroys insulation of signal and promotes conduction of signal among cells, effectively destroying insulating phases

In the absence of noise, the secrete-and-sense cells can operate in the autonomy phase (Fig. 1b - yellow region). In this phase, every spatial configuration is a steady state. Noise can remove this phase. To see this, note that by equation S21:

$$Y_i^{\text{nei}} = f(a_0)\left[(C_{ON}-1)\,m_i + 6\right] + \left(f_N - 6f(a_0)\right)\left[pC_{ON} + (1-p)\right] \tag{S110}$$

Suppose that the noise strength is larger than the minimum required noise strength for perturbing the system (equation S107). Consider an ON-cell. If none of its nearest neighbours are ON, the signal concentration on this cell due to all the other cells is too low so the α_{min} (equation S107) cannot be satisfied. Thus this ON-cell is very likely to be affected by noise. On the other hand if this cell has most of its nearest neighbours (and potentially its second- and third-neighbours) ON, then Y_i^{nei} is higher and the probability that the cell will stay ON is high. A similar argument applies to OFF-cells. Therefore, if the noise in the system satisfies the conditions discussed in section S7, the autonomy phase cannot be sustained and the cellular lattice tends to form clusters of ON- and OFF-cells. Moreover, in the limit of infinitely long time, all cells will have turned ON or OFF.

S7.5-b. Effect of noise-induced conduction of signal among cells in various phases of the secrete-and-sense cells

Recall that the activate-deactivate phase replaces the autonomy phase when the interaction strength f_N becomes larger than the critical strength (i.e. $f_N(a_0) > 1$) and that the multicellular entropy (from Maire and Youk, *Cell Systems* (2015)) is maximized in the activate-deactivate phase. Recall also that in the activate-deactivate phase, the deterministic secrete-and-sense cells, depending on $p(t=0)$, behaves as activating (if $p(t=0) > p_c$: blue paths in Fig. 3d), deactivating (if $p(t=0) < p_c$: red paths in Fig. 3d), or autonomous (if $p(t=0) \approx p_c$: brown paths in Fig. 3d) (Note that $p_c \approx 0.5$ in Fig. 3d). The deterministic secrete-and-sense cells in the activate-deactivate phase with $p(t=0) \approx p_c$ behave like autonomy cells. If we add noise to these secrete-and-sense cells, p can increase in the first few time steps, leading to the cells behaving as if they are in the activate phase (Fig. 3d - some brown streamlines move like the blue streamlines). Similarly, noise can also decrease the p in the first few time steps, causing the cells to behave as if they are in the deactivate phase (Fig. 3d - some brown streamlines move like the red streamlines). Therefore we expect that spatial configurations are more stable if the pseudo-energy landscape that has a "broad" enough shape in which fluctuations in p above and below p_c does not push the particle (cellular lattice) down a steep gradient in the landscape. We can also apply this idea to the autonomy phase. Consider the pseudo-energy landscapes of two deterministic cellular automata that both operate in the autonomy phase (Fig. S9). One of them has a symmetric pseudo-energy landscape (Fig. S9A) and the other has a skewed (asymmetric) pseudo-energy landscape (Fig. S9B). Now we add noise to both cellular automata. For both pseudo-energy landscapes, we find that the particles get stuck in metabstable states with higher spatial order than what they started with (Fig. S9). Recall that in the autonomy phase, without noise, there is no dynamics - cells end up with the spatial index that they started with. But the stability of the metastable states depend on the shape of the pseudo-energy landscape. Namely, when the pseudo-energy landscape is symmetric around the peak (Fig. S9A), as the particle rolls down the landscape from $(p(t=0) \approx p_c, I(t=0) \approx 0)$, it has an almost equal

chance of moving to the right (i.e. $p > p_c$) as it does to the left or to the left (i.e. $p < p_c$) due to noise (Fig. S9A - red paths). Thus the particle tends to stay with $p \approx p_c$ throughout its motion. This means that the spatial configuration becomes more organised and tends to remain organised for longer a longer time than when the pseudo-energy landscape is asymmetrical. On the other hand, when the pseudo-energy landscape is skewed towards one side, for example towards $p = 0$ (Fig. S9B), noise tends to decrease the particle's p as in the deactivate phase, but now at a slower rate than in the deterministic deactivate phase.

S7.5.c. Stability and stochastic dynamics of noisy secrete-and-sense cells that yield disorder-to-order transitions

In the absence of noise, a steady state spatial configuration is one in which no cell changes its state at the next time step. With noise, this is not possible because any spatial configuration can be changed by the noise given sufficient number of time steps. Therefore, we need a definition of stability to determine when we can terminate a noisy cellular automaton without worrying that we miss important features in the dynamics that could occur at the next time steps. We define stability as follows:

If the standard deviation in p during Q time steps is less than δp and the standard deviation in I during the same Q time steps is less than δI, then the spatial configuration is stable.

S8 Extension to multiple cell-types and multiple signal-types: A proof of principle

In this section, we extend our to lattices composed of multiple types of cells that communicate through more than one type of signal.

S8.1 General framework for lattices with an arbitrary number of cell types and an arbitrary number of signals

We consider L types of cells on a lattice that interact through M types of signalling molecules (signals). Cells of different types have different radii (R). Each cell type may secrete and sense different types of signal. Each signal would have its own diffusion length λ. Each cell type might have its own genetic circuit parameters, C_{ON}, C_{OFF} and K. The different values of λ and R would mean that the interaction term f_{ij} between cell-i and cell-j - two cells that could be of different types - can be non-trivial. We can represent cell-cell interactions by an **interaction matrix** M, that we define similarly as in equation S10, but now with its off diagonal elements assuming non-trivial forms that depend on the cell types that exist on the lattice. Suppose we have L cell types on a triangular lattice. Each cell type-l has genetic circuit parameters - $C_{OFF,l}$, $C_{ON,l}$ and K_l. Without loss of generality, we assume that all concentrations are measured in units of $C_{OFF,1}$, and hence $C_{OFF,l} = 1$.

In the following analysis, we will use the vector notation that we introduced in section S1 but now we order the vectors to group cells of the same type together. Then the vector $\vec{X}$ that represents each cell's state (-1 if OFF and $+1$ if ON) has the following structure:

$$\vec{X} = \begin{pmatrix} \vec{X}_{i\in 1} \\ \hline \vdots \\ \hline \vec{X}_{i\in l} \\ \hline \vdots \\ \hline \vec{X}_{i\in L} \end{pmatrix} \tag{S111}$$

where the dimension of each sub-vector $\vec{X}_{i\in l}$ is equal to the number N_l of cells of type l. The dimension of $\vec{X}$ is thus N where $\sum_{l=0}^{L} N_l = N$.

Similarly, we define a vector $\vec{K}$ of activation thresholds as

$$\vec{K} = \begin{pmatrix} K_1 \\ \vdots \\ K_1 \\ \hline \vdots \\ \hline K_l \\ \vdots \\ K_l \\ \hline \vdots \\ \hline K_L \\ \vdots \\ K_L \end{pmatrix} \tag{S112}$$

where each K_l is repeated N_l times. Finally we define a vector $\vec{Y}_{\text{self}}$ of self-contributed signal concentrations as

$$\vec{Y}_{\text{self}} = \begin{pmatrix} \frac{1}{2}(C_{ON,1}-1)\vec{X}_{i\in 1} + \frac{1}{2}(C_{ON,1}+1)\vec{1}_{N_1} \\ \hline \vdots \\ \hline \frac{1}{2}(C_{ON,l}-C_{OFF,l})\vec{X}_{i\in l} + \frac{1}{2}(C_{ON,l}+C_{OFF,l})\vec{1}_{N_l} \\ \hline \vdots \\ \hline \frac{1}{2}(C_{ON,L}-C_{OFF,L})\vec{X}_{i\in L} + \frac{1}{2}(C_{ON,L}+C_{OFF,L})\vec{1}_{N_L} \end{pmatrix} \tag{S113}$$

where $\vec{1}_{N_l}$ is a vector of ones of dimension N_l. $\vec{Y}_{\text{self}}$ is the concentration sensed by each cell due to its own secretion, and represents secrete-and-sense (autocrine) part of signalling. Therefore, given a state $\vec{X}$ in the system, we can calculate the signal concentrations sensed by each cell as

$$\vec{Y} = M\vec{Y}_{\text{self}} \tag{S114}$$

where the matrix M. Now we can split M in the following way:

$$M = \left(\begin{array}{c|c|c|c|c} M^{11} & \dots & M^{1m} & \dots & M^{1L} \\ \hline \vdots & \vdots & \vdots & \vdots & \vdots \\ \hline M^{l1} & \dots & M^{lm} & \dots & M^{lL} \\ \hline \vdots & \vdots & \vdots & \vdots & \vdots \\ \hline M^{L1} & \dots & M^{Lm} & \dots & M^{LL} \end{array}\right) \tag{S115}$$

where the sub-matrices M^{lm} have a dimension $N_l \times N_m$. Each entry of M^{lm} is an interaction term for a pair of cells, one of which is of type l and the other is of type m:

$$[M^{lm}]_{ij} = M_{i\in l, j\in m} \equiv f_{ij}^{lm} \tag{S116}$$

If, for instance, cells of type l and cells of type m do not interact because they cannot sense each others' signals (i.e., they lack the corresponding receptors), then we have $f_{ij}^{lm} = 0$.

Using the above notation, the cellular automaton simulation proceeds by updating each cell's state through the following rule:

$$\vec{X}_{t+1} = \text{sgn}\left(\vec{Y}_t - \vec{K}\right) \tag{S117}$$

where the function $\text{sgn}(\vec{A})$ takes the sign of the each element and returns $+1$ if the element is positive and -1 if the element is negative.

Given a vector $\vec{X}$ that determines the state of a system, the total concentration of all signals on a cell-i of type l ($i \in l$) is

$$Y_{i\in l} = \frac{1}{2}(C_{ON,l}-C_{OFF,l})X_i+\frac{1}{2}(C_{ON,l}+C_{OFF,l})+\sum_{m=1}^{L}\sum_{\substack{j\in m\\ j\neq i}} f_{ij}^{lm}\left[\frac{1}{2}(C_{ON,m}-C_{OFF,m})X_j+\frac{1}{2}(C_{ON,m}+C_{OFF,m})\right] \tag{S118}$$

S8.1-a. Behavioural phases

Let us now determine the phases of a lattice with L cell types and M signals. We will find that the phase diagram is now multidimensional (instead of being two-dimensional as in Fig. 1b) because we now have more than two genetic circuit parameters (when $L > 1$) and the interaction strength is now characterised a matrix (i.e., the interaction matrix M) rather than by the scalar function f_N. Let us begin by analysing the case of all cells of type l being always ON. This occurs if

$$Y_{i\in l} = C_{OFF,l} + \sum_{m=1}^{L}\sum_{\substack{j\in m\\ j\neq i}} f_{ij}^{lm} C_{OFF,m} > K_l \tag{S119}$$

We note that the terms f_{ij}^{lm} are not the same for all cells of the same type. The condition that ensures all the cells of type l to be always ON is then:

$$C_{OFF,l} + \sum_{m=1}^{L} C_{OFF,m} \max\left(\sum_{\substack{j\in m\\ j\neq i}} f_{ij}^{lm}\right) > K_l \tag{S120}$$

Similarly, the condition that ensures all cells of type l to be OFF is

$$C_{ON,l} + \sum_{m=1}^{L} C_{ON,m} \min\left(\sum_{\substack{j\in m\\ j\neq i}} f_{ij}^{lm}\right) < K_l \tag{S121}$$

We can also find the following condition that ensures a cell of type l that is ON to remain ON:

$$C_{ON,l} + \sum_{m=1}^{L} C_{OFF,m} \max\left(\sum_{\substack{j\in m\\ j\neq i}} f_{ij}^{lm}\right) > K_l \tag{S122}$$

and a condition that ensures a cell of type l that is OFF to remain OFF:

$$C_{OFF,l} + \sum_{m=1}^{L} C_{ON,m} \min\left(\sum_{\substack{j\in m\\ j\neq i}} f_{ij}^{lm}\right) < K_l \tag{S123}$$

If we define a 3L-dimensional space spanned by $\{C_{ON,l}, C_{OFF,l}, K_l\}$, then equations S120-S123 define hyperplanes in this space, which represent boundary manifolds between different phases, that are analogous to the phase boundary lines that we obtained for phase diagrams of lattices of identical secrete-and-sense cells (Fig. 1b). But unlike the phase diagrams for lattices of identical secrete-and-sense cells (Fig. 1b), the phases for L type of cells and M signal types now depend on the spatial arrangement of the different cell types on a lattice as well as the interaction strengths.

S8.1-b. Multicellular entropy

To calculate the multicellular entropy for a lattice with L cell types, we follow an approach similar to that outlined in Maire and Youk (*Cell Systems* (2015)). We consider picking a random configuration of ON- and OFF-cells from an ensemble of spatial configurations and calculate the probability that each ON- and OFF-cell will remain in the same state at the next time step. The combined probability of all cells remaining in the same state gives the probability that the randomly picked configuration is a steady state spatial configuration. However, there is a caveat. Instead of a single value of p (fraction of cells that are ON), we now have multiple values of p, one for each cell type. If there are n_l ON-cells of type l, we define $p_l = n_l/N_l$. The total number of steady state configurations, given a macrostate state $\{p_1, ..., p_l, ..., p_L\}$, is

$$\Omega_{p_1,...,p_l,...,p_L} = P_{eq}(p_1, ..., p_l, ..., p_L) \prod_{l=1}^{L} \binom{N_l}{Np_l} \tag{S124}$$

and the total number of steady states is thus

$$\Omega = \sum_{\substack{\text{All combinations of} \\ \{p_1,...,p_l,...,p_L\}}} P_{eq}(p_1, ..., p_l, ..., p_L) \prod_{l=1}^{L} \binom{N_l}{Np_l} \tag{S125}$$

To calculate $P_{eq}(p_1, ..., p_l, ..., p_L)$, we use a mean-field approach (Appendix A) and assume that the concentrations of the signals due to all the other cells is normally distributed among the cells because it is given by the weighted sum of the self-contributed concentrations of the signals:

$$Y_{i\in l}^{\text{nei}} = \sum_{m=1}^{L} \sum_{\substack{j\in m \\ j\neq i}} f_{ij}^{lm} \left[\frac{1}{2}(C_{ON,m} - C_{OFF,m})X_j + \frac{1}{2}(C_{ON,m} + C_{OFF,m}) \right] \tag{S126}$$

To calculate the average concentration of the signals due to all the other cells, we use

$$\mu_l = \frac{1}{N_l} \sum_{i\in l} Y_{i\in l}^{\text{nei}} = \frac{1}{N_l} \sum_{i\in l} \sum_{m=1}^{L} \sum_{\substack{j\in m \\ j\neq i}} f_{ij}^{lm} \left[\frac{1}{2}(C_{ON,m} - C_{OFF,m})X_j + \frac{1}{2}(C_{ON,m} + C_{OFF,m}) \right] \tag{S127}$$

We now define the **average interaction strength of cells of type l on cells of type m** (and vice-versa since M is symmetric) as the sum over all the elements of M^{lm} except for those that are diagonal elements of M:

$$f_{lm} \equiv \frac{1}{N} \sum_{i\in l} \sum_{\substack{j\in m \\ j\neq i}} f_{ij}^{lm} \tag{S128}$$

We use above to calculate the average concentration of the signals on each cell of type l due to all the other cells:

$$\mu_l = \frac{N}{N_l} \sum_{m=1}^{L} f_{lm} \left[(C_{ON,m} - C_{OFF,m})p_m + C_{OFF,m} \right] \tag{S129}$$

Proceeding in the same way for the variance, we define

$$g_{lm} \equiv \frac{1}{N} \sum_{i\in l} \sum_{\substack{j\in m \\ j\neq i}} \left(f_{ij}^{lm}\right)^2 \tag{S130}$$

and assuming that the states X_i of each cell are independent of each other, we have

$$\sigma_l^2 = \frac{N}{N_l} \sum_{m=1}^{L} g_{lm}(C_{ON,m} - C_{OFF,m})^2 p_m(1 - p_m) \tag{S131}$$

We can now define the probabilities that cells of type l will keep their states in the next time step,

$$P_{ON\to ON;l} = 1 - D\left(K_l - C_{ON,l}; \mu_l, \sigma_l\right) = \frac{1}{2}\left[1 - \text{erf}\left(\frac{K_l - C_{ON,l} - \mu_l}{\sqrt{2}\sigma_l}\right)\right] \tag{S132a}$$

$$P_{OFF\to OFF;l} = D\left(K_l - C_{OFF,l}; \mu_l, \sigma_l\right) = \frac{1}{2}\left[1 + \text{erf}\left(\frac{K_l - C_{OFF,l} - \mu_l}{\sqrt{2}\sigma_l}\right)\right] \tag{S132b}$$

and use these probabilities calculate the total number of steady states:

$$\Omega = \sum_{\substack{\text{All combinations of} \\ \{p_1,\ldots,p_l,\ldots,p_L\}}} \prod_{l=0}^{L} P_{ON\to ON;l}^{N_l p_l} P_{OFF\to OFF;l}^{N_l(1-p_l)} \binom{N_l}{N p_l} \tag{S133}$$

Note that this approach is general and works with any interaction matrix elements f_{ij}. For instance, if cells of distinct types do not interact with each other, we have $f_{lm} = 0$ when $l \neq m$. Furthermore, if cells of distinct types interact very weakly compared to the interactions among cells of the same type, then $f_{lm} << f_{ll}$ for $l \neq m$. We can apply our approach here to any interaction strengths, no matter how complex the interactions are.

S8.1-c. Interaction matrix

Let us examine closely the meaning of the interaction matrix in the case of multiple cell types. For this purpose, we assume that cells all communicate using the same signal and have the same radius. In other words, we consider L types of secrete-and-sense cells that use the same signal. The cell types differ in their values of C_{ON}, C_{OFF}, and K. Thus the components $f(r_{ij})$ of the interaction matrix M still have the same form as in Section S1.

In this particular system, as more cells of type l are located, on average, further away from cells of type m, the smaller the f_{lm} becomes. However, if f_{lm} becomes smaller, then the interaction strength from the other cell types would compensate the decrease in f_{lm}. Specifically,

$$\sum_{l=1}^{L}\sum_{m=1}^{L} f_{lm} = f_N \tag{S134}$$

Another feature of the interaction matrix element f_{lm} is that it usually becomes larger as the number of cells of type l and m increases.

Suppose now that we have two different types of secrete-and-sense cells that use the same signal. Let us also assume that these cells, of types 1 and 2, are randomly arranged in space. We can then estimate the interaction matrix elements for cell types 1 and 2 by noting that, in this case, the interaction strengths are approximately evenly distributed in the matrix M, which leads to

$$f_{lm} \approx \frac{N_l N_m}{N^2} f_N \tag{S135}$$

As an example, consider the randomly distributed configuration ($N_1 = N_2 = 200$). Since $f_N = 2.358$, equation S135 tells us that $f_{11} = f_{22} = f_{12} = 0.5895$, which closely match the value obtained by an exact calculation. Doing the same for another configuration ($N_1 = 100$ and $N_2 = 300$), equation S135 tells us that $f_{11} = 0.147$, $f_{12} = 0.442$ and $f_{22} = 1.326$.These also closely match the values obtained by an exact calculation.

S8.2 Modified pseudo-energy and spatial index

In this section, we extend the pseudo-energy H to an arbitrary number of cell types. Analogous to the case of one cell type, we can define, for a lattice with L cell types,

$$H = -\vec{X}\cdot(\vec{Y} - \vec{K}) = -\sum_{l=1}^{L}\sum_{i\in l} X_i(Y_i - K_l) \tag{S136}$$

Using equation S118 we can rewrite H as

$$h \equiv \frac{H}{N} = -\sum_{l=1}^{L}\left\{\frac{N_l}{N}\left[p_l C_{ON,l} - (1-p_l)C_{OFF,l} - K_l(2p_l-1)\right]\right.$$
$$\left. + \sum_{m=1}^{L}\left[\frac{C_{ON,m}}{2}(\theta_{lm} + (2p_l-1)f_{lm}) - \frac{C_{OFF,m}}{2}(\theta_{lm} - (2p_l-1)f_{lm})\right]\right\} \tag{S137}$$

where we have defined a **new measure for the spatial order θ_{lm} among cells of types l and m**:

$$\theta_{lm} = \frac{1}{N}\sum_{i\in l}\sum_{\substack{j\in m \\ j\neq i}} f_{ij}^{lm} X_i X_j \tag{S138}$$

This suggests that for a lattice with L cell types, the description of the system can be given by $\frac{L(L+3)}{2}$ variables. The L-dimensional set $\{p_1, \ldots, p_L\}$ describes the fraction of cells that are ON and the $\frac{L(L+1)}{2}$-dimensional set $\{\theta_{11}, \ldots, \theta_{1L}, \theta_{22}, \ldots, \theta_{2L}, \theta 33, \ldots, \theta_{(L-1)L}, \theta_{LL}\}$ describes the spatial order among cells of different types.

To make a parallel with spin systems, we can rewrite equation S137 as

$$H' \equiv H + \sum_{l=1}^{L}\frac{N_l}{2}\left(C_{ON,l} - C_{OFF,l}\right)$$
$$= -\sum_{l=1}^{L}\sum_{i\in l} X_i\left[\frac{C_{ON,l}+C_{OFF,l}}{2} - K_l + \frac{N}{N_l}\sum_{m=1}^{L}\frac{C_{ON,m}+C_{OFF,m}}{2}f_{lm}\right] - N\sum_{l=1}^{L}\sum_{m=1}^{L}\theta_{lm} \tag{S139}$$

and we see that we can split the pseudo-energy for each cell type as

$$H' = \sum_{l=1}^{L} H_l = -\sum_{l=1}^{L}\left[B_l\sum_{i\in l} X_i + N\Theta_l\right] \tag{S140}$$

using the following definitions

$$B_l = \frac{C_{ON,l}+C_{OFF,l}}{2} - K_l + \frac{N}{N_l}\sum_{m=1}^{L}\frac{C_{ON,m}+C_{OFF,m}}{2}f_{lm} \tag{S141}$$

$$\Theta_l = \sum_{m=1}^{L}\theta_{lm} = \frac{1}{N}\sum_{m=1}^{L}\sum_{i\in l}\sum_{\substack{j\in m \\ j\neq i}} f_{ij}^{lm} X_i X_j \tag{S142}$$